12/5-18-92 8S ①

PNL-8076
UC-313

Inert Electrodes Program

Final Report on DSA Methods for Monitoring Alumina in Aluminum Reduction Cells with Cermet Anodes

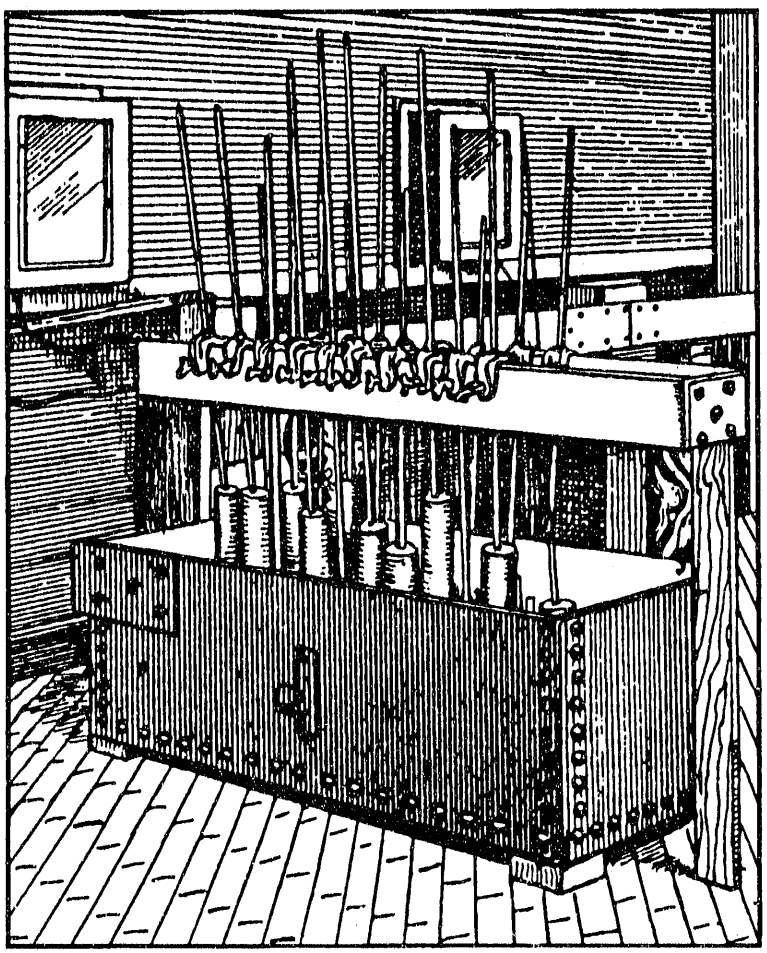

April 1992

Work Supported by the U.S. Department of Energy
under Contract DE-AC06-76RLO 1830

Pacific Northwest Laboratory
Operated for the U.S. Department of Energy
by Battelle Memorial Institute

Battelle

PNL-8076

DISTRIBUTION OF THIS DOCUMENT IS UNLIMITED

DISCLAIMER

This report was prepared as an account of work sponsored by an agency of the United States Government. Neither the United States Government nor any agency thereof, nor Battelle Memorial Institute, nor any of their employees, makes **any warranty, expressed or implied, or assumes any legal liability or responsibility for the accuracy, completeness, or usefulness of any information, apparatus, product, or process disclosed, or represents that its use would not infringe privately owned rights.** Reference herein to any specific commercial product, process, or service by trade name, trademark, manufacturer, or otherwise does not necessarily constitute or imply its endorsement, recommendation, or favoring by the United States Government or any agency thereof, or Battelle Memorial Institute. The views and opinions of authors expressed herein do not necessarily state or reflect those of the United States Government or any agency thereof.

PACIFIC NORTHWEST LABORATORY
operated by
BATTELLE MEMORIAL INSTITUTE
for the
UNITED STATES DEPARTMENT OF ENERGY
under Contract DE-AC06-76RLO 1830

Printed in the United States of America

Available to DOE and DOE contractors from the Office of Scientific and Technical Information, P.O. Box 62, Oak Ridge, TN 37831; prices available from (615) 576-8401. FTS 626-8401.

Available to the public from the National Technical Information Service, U.S. Department of Commerce, 5285 Port Royal Rd., Springfield, VA 22161.

PNL--8076

DE92 013599

Inert Electrode Program

FINAL REPORT ON DSA METHODS FOR MONITORING ALUMINA IN ALUMINUM REDUCTION CELLS WITH CERMET ANODES

C. F. Windisch, Jr.

April 1992

Prepared for
the U.S. Department of Energy
under Contract DE-AC06-76RLO 1830

Pacific Northwest Laboratory
Richland, Washington 99352

MASTER

ACKNOWLEDGMENTS

The author wishes to acknowledge the technical assistance of N. D. Stice, N. C. Davis, and R. E. Williford, Pacific Northwest Laboratory; the assistance with DSA analysis and many fruitful discussions by C. L. Nikias, University of Southern California, Los Angeles, California, the programmatic support provided by M. J. McMonigle and the Office of Industrial Processes, U.S. Department of Energy (DOE), Washington, D. C., and the DOE Richland Field Office. The author is also grateful to the personnel at Reynolds Metals Company, Sheffield, Alabama, who assisted in performing the prototype anode test in March 1989 and the pilot cell test in August 1991.

SUMMARY

After numerous analyses of digital voltage and current data collected from laboratory cells and a pilot-scale cell, it is still not clear whether any of the quantification parameters computed from the signals are suitable as the basis for an alumina sensor. Many different quantification parameters were studied and these showed varied behavior for both the laboratory and pilot-scale studies, but no consistent correlation of any of these parameters with alumina concentration was observed. There are two possible explanations for the lack of consistent correlation involving the signal parameters: 1) there was no dependence, or a very weak one, on alumina concentration, and/or 2) there were overriding factors or extraneous noise that reduced the sensitivity or "overwhelmed" the signal components effected by alumina concentration. It is recommended that further study using digital signal analysis methods be suspended or postponed until a less "noisy" pilot-scale test is performed with cermet anodes or until a new strategy is developed for applying the approach, for example, to carbon anodes in commercial cells where a significantly greater volume of data can be collected over much longer periods.

CONTENTS

ACKNOWLEDGMENTS iii

SUMMARY v

1.0 INTRODUCTION 1.1

2.0 PROCEDURES 2.1

2.1 LABORATORY CELL TESTS 2.1

2.2 PILOT CELL TEST 2.3

2.3 DSA METHODS 2.9

3.0 RESULTS OF ANALYSIS 3.1

3.1 LABORATORY CELL TESTS 3.1

3.1.1 Variations with Alumina Concentration 3.1

3.1.2 Variations with Current Density 3.5

3.1.3 The Frequency Spectrum and Sensitivity 3.7

3.1.4 Variations with ACD 3.8

3.2 PILOT CELL TEST 3.12

4.0 CONCLUSIONS AND RECOMMENDATIONS 4.1

5.0 REFERENCES 5.1

APPENDIX: DIGITAL SIGNAL ANALYSIS METHODS A.1

FIGURES

2.1 Apparatus for PNL Laboratory Tests 2.2

2.2 Arrangement of Anodes in the Pilot Cell Test 2.5

2.3a Block Diagrams Showing Wiring of Data Acquisition System for the Pilot Cell Test 2.6

2.3b Block Diagrams Showing Physical Setup of Data Acquisition System for the Pilot Cell Test 2.7

2.4 Variation of the Alumina Concentration with Time during the Pilot Cell Test 2.9

2.5 Variation in Current Through Anode in Position A during the Pilot Cell Test 2.10

2.6 Variation in Current Through Anode in Position B during the Pilot Cell Test 2.10

2.7 Variation in Current Through Anode in Position C during the Pilot Cell Test 2.11

2.8 Variation in Current Through Anode in Position D during the Pilot Cell Test 2.11

2.9 Variation in Current Through Anode in Position E during the Pilot Cell Test 2.12

2.10 Variation in Current Through Anode in Position F during the Pilot Cell Test 2.12

3.1 Plot of Conductance, L, by Cross-Correlation versus Weight Percent Alumina at Various Current Densities 3.3

3.2 Plot of COEF2 versus Weight Percent Alumina at Various Current Densities 3.3

3.3 Plot of COEF6 versus Weight Percent Alumina at Various Current Densities 3.4

3.4 Plots of L, COEF2 and COEF6 versus Weight Percent Alumina for SET#3 Data 3.6

3.5 Plot of COEF2 versus Current Density for Various Alumina Concentrations 3.7

3.6 Comparison of Conductance versus Weight Percent Alumina Data a) With and b) Without a 25 Hz Low-Pass Filter 3.8

3.7 Plot of Conductance versus ACD for Various Alumina Concentrations 3.11

3.8 Typical Current and Voltage-versus-Time Plots for the Pilot Cell Test Data 3.12

3.9 Comparison of L and Alumina Concentration as a Function of Time during the Pilot Cell Test for Anode in Position D . . . 3.15

3.10 Comparison of L and Alumina Concentration as a Function of Time during the Pilot Cell Test for Anode in Position F . . . 3.17

3.11 Correlation Plot for Anode in Position F with the Large Carbon Anode 3.17

TABLES

2.1 Pilot Cell Test DSA Data Files 2.13

1.0 INTRODUCTION

The Sensors Development Program was conducted at the Pacific Northwest Laboratory (PNL)[a] for the U.S. Department of Energy, Office of Industrial Processes. The work was performed in conjunction with the Inert Electrodes Program at PNL. The objective of the Sensors Development Program in FY 1990 through FY 1992 was to determine whether methods based on digital signal analysis (DSA) could be used to measure alumina concentration in aluminum reduction cells. Specifically, this work was performed to determine whether useful correlations exist between alumina concentration and various DSA-derived quantification parameters, calculated for current and voltage signals from laboratory and field aluminum reduction cells. If appropriate correlations could be found, then the quantification parameters might be used to monitor and, consequently, help control the alumina concentration in commercial reduction cells. The control of alumina concentration is especially important for cermet anodes, which have exhibited instability and excessive wear at alumina concentrations removed from saturation.

A subcontract was written to Dr. C. L. Nikias, Professor, University of Southern California, Los Angeles, California, to assist in developing DSA-based methods by analysis of data from PNL laboratory tests and the pilot cell test of the cermet anodes. In FY 1989 and FY 1990, Dr. Nikias completed studies on PNL laboratory data for various current densities and alumina concentrations and on data collected during the prototype anode test. These results were discussed in a previous PNL report (Windisch et al. 1990). The present report focuses on the results of additional analyses using laboratory cells in FY 1990 and the pilot cell in FY 1991 and FY 1992.

The principal result discussed in Windisch et al. (1990) was that the relationship between selected DSA quantification parameters and current density for data collected from laboratory cells showed a trend that was consistent with data from the prototype anode test. This result suggested that laboratory cells were a reliable "proving ground" for the development of a

---

(a) Operated for the U.S. Department of Energy by Battelle Memorial Institute under Contract DE-AC06-76RLO 1830.

commercial DSA-based sensor. The dependency on current density, however, while interesting in its own right and possibly indicative of the mechanisms of the various anode properties/reactions, was not sufficiently refined to serve as a basis for a viable sensor. The current density dependency was weak at current densities at or below 1.0 A/cm^2, suggesting that either improvement in analytical sensitivity or a change in experimental procedure was warranted. Since alumina concentration is one of the main cell conditions for which a sensor is required, ultimately the dependency needed to be related to alumina concentration. But the alumina concentration dependency was unacceptable, showing significant sensitivity only between 20% and 40% of saturation. Clearly, further work was required to advance these or other preliminary parameter correlations to a stage where they could be useful for a DSA-based sensor.

The work summarized in this report was aimed at determining whether a more sensitive and reliable relationship between a DSA quantification parameter and alumina concentration could be found. Toward this end, both additional laboratory data were collected and a pilot-scale test was performed. Laboratory cell data were collected over a wider range of operating conditions than previously. The effects of varying current density/cell potential and anode-to-cathode distance (ACD) were studied in addition to varying alumina concentration. Alternating potential "ripples" were also applied to the controlling voltage to determine the sensitivity of parameters related to electrochemical impedance. In all, over three hundred different combinations of these conditions were tested in the laboratory. In addition to widening the range of operating conditions, other DSA approaches were also attempted by Dr. Nikias and these are discussed in the Appendix. In August 1991, a pilot-scale test of the cermet anodes was performed at the Reynolds Metals Company (RMC) facility in Sheffield, Alabama. Current and voltage signals were collected during this test, and later were subjected to the same analyses as the laboratory data (i.e., for possible correlation with alumina concentration). The objective of using the pilot cell data was to corroborate the finding of the laboratory cell tests and/or further demonstrate whether scale-up significantly influenced any correlations that were observed in the laboratory cells.

PNL also has performed digital signal analysis on data from laboratory cells and the pilot cell using methods from chaos theory. The results of the work using chaos theory are being presented in a separate report.

2.0 PROCEDURES

2.1 LABORATORY CELL TESTS

The PNL laboratory cell used to collect the data discussed in this report is shown in Figure 2.1. An IBM AT computer containing an Analog Devices, Inc., RTI-860 high-speed simultaneous analog input board connected to Analog Devices 3B40-00 and 3B41-00 isolation amplifiers was used with the HEM Data Corporation Snapshot Storage Scope software to collect, display, and store the data. The inputs to the IBM AT were current and voltage signals taken from a PAR 173 potentiostat that was operated in the potentiostatic (potential control) mode in these experiments. The electrochemical cell was similar to that used in previous sensors development work at PNL. It consisted of a graphite crucible that served as the cathode and a BN-sheathed cermet electrode as the anode. No reference electrode was employed. The best configuration for reducing instrumental noise was to operate the cathode as the working electrode. Consequently, in this work, the working electrode terminal was connected to the cathode and the counter and reference electrode terminals were connected to the anode. To compensate for this "reverse" configuration, the potential was set at negative potentials in order to drive the cermet electrode anodically. The exposed surface area of the anode was 1 cm^2. The initial bath was prepared by mixing appropriate amounts of reagent grade materials to give a bath ratio equal to 1.15, 5.5% (by weight) CaF_2, 1.0% MgF_2, and the desired concentration of alumina. A temperature controller/furnace/thermocouple was used to control the bath temperature at 983°C. Bath ratio and temperature were effectively constant throughout these short-term experiments. In a given test, the anode was inserted once the bath had become molten, the temperature was allowed to reequilibrate, then the anode was polarized potentiostatically to give the desired current density.

Current and voltage signals were collected for cells with different alumina concentrations, cell voltage/anode current densities, and anode-to-cathode distances (ACD). These tests were labeled the "ACD tests." Every combination of the following nominal values for these parameters was tested:

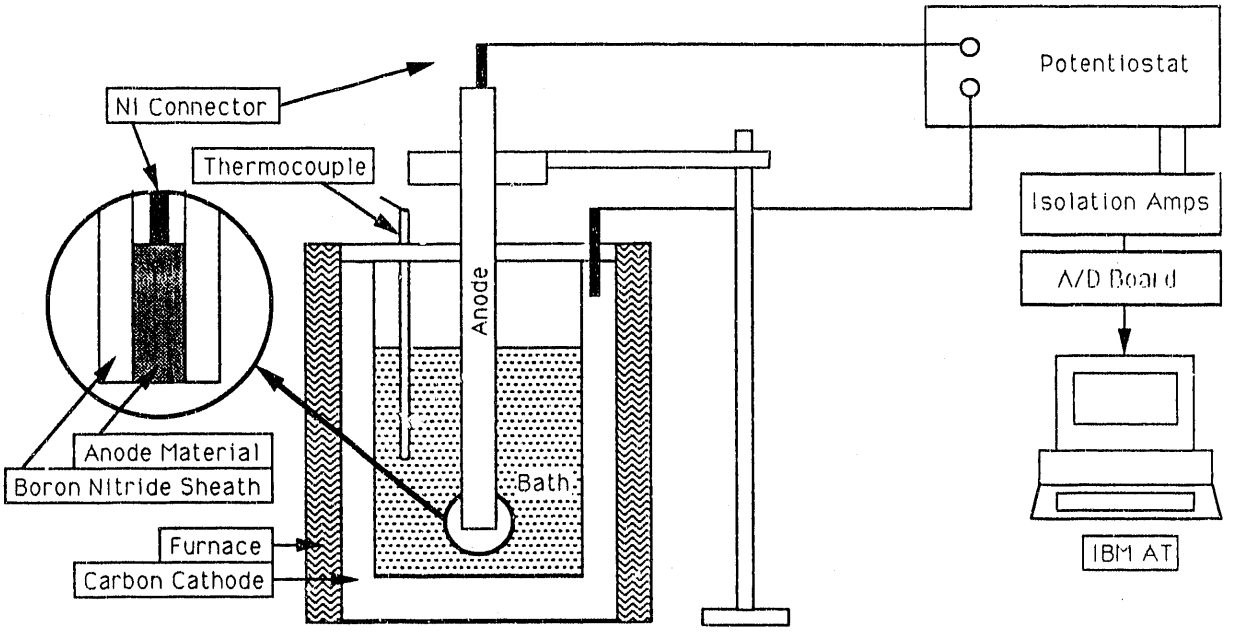

FIGURE 2.1. Apparatus for PNL Laboratory Tests

Alumina Concentration (weight percent): 0%, 1.5%, 3.0%, 4.5%, 5.1%, 5.6%, and 6% (where 8 wt% is approximately saturation).

Current Density (A/cm^2): 0.25, 0.50, 0.75, and 1.0.

ACD (in.): 3, 2.25, 1.5, and 0.75.

Data for a given set of conditions consisted of 10,000 sequential signals collected over a period of 0.5 s (20 kHz sampling frequency). The digital signals were stored as files on 1.4 MB floppy disks. In addition, for each set of conditions, one file was collected without any additional voltage signal applied and two files with an ±10 mV AC "ripple" superimposed on the controlling voltage. The frequencies of the ripples were 10 Hz and 1 kHz. These ripple tests were performed to facilitate impedance calculations that may be appropriate in the analysis.

Another set of data was also collected. These data, labeled the "DSA tests," completed the data sets with conditions closer to alumina saturation

and over a wider range of alumina concentrations. They employed a ±50 mV ripple instead of the ±10 mV ripple per a request by Dr. Nikias as a possible way to improve sensitivity. The nominal conditions for the DSA tests were the following:

Alumina Concentration (weight percent): 4.0%, 4.4%, 4.8%, 5.2%, 5.6%, 6.0%, 6.4%, 6.8%, 7.2%, 7.6%, and 8.0%.

Current Density (A/cm^2): 0.5 and 0.66.

ACD (in.): 1.5 only.

Similar to the ACD tests, for each set of conditions one file was collected without any additional voltage signal applied and two files with the ±50 mV ripple as previously indicated, at frequencies of 5 and 10 Hz. In addition, another set of files was collected on a standard 2-ohm resistor to determine the extent of instrumental noise. The resistor data were collected at 0.5 and 1.0 A.

To address some ambiguities in the results from the above data (discussed in Section 3.1.1), one more set of laboratory data were collected and analyzed. These data, called "Set#3," were collected under conditions similar to those reported above but only at 0.5 and 0.75 A/cm^2 and with the ACD = 1.5 in. Data were collected at 13 different alumina concentrations between 0 and 8 wt%. Similar to previous experiments, data files were collected with no AC ripple applied and with an applied ±10 mV signal at 10 Hz.

2.2 PILOT CELL TEST

The pilot cell test of the cermet anodes was performed between August 10 and August 30, 1991, at the RMC facility in Sheffield, Alabama. The pilot cell is a small, self-heated, aluminum reduction cell with the capacity for running two "large" (industrial-size) carbon anodes. During the pilot cell test, thirteen (13) cermet anodes were tested in a six-pack cluster (using a predetermined exchange sequence) which was inserted in one of the two large

anode positions.[a] A single large carbon anode was run in conjunction with a six-pack cluster in the remaining position. The cermet anodes had the same composition as those evaluated in the laboratory experiments but were manufactured by Ceramic Magnetics, Inc., Fairfield, N.J.

The arrangement of the carbon anode and the cermet anode cluster is shown in Figure 2.2. The cermet anode cluster consisted of six cermet anodes with positions denoted as A through F. The cermet anodes were roughly cylindrical with a radius of about 3 in. and a height of 3 in. in the center, with an additional 1-inch lip on the upper edge. All edges were rounded to reduce corner effects.

The pilot cell power supplies were essentially unfiltered DC (actually, 6-phase rectified AC) output units capable of thousands of amps in the 5 to 10 V range. The supplies "floated" with respect to building electrical ground, so common mode voltages existed that were not controlled. The pilot cell voltage and current signals were derived from dividers and shunts connected directly to the pilot cell, and so floated with it. This electrically noisy environment and the heat generated by the pilot cell during operation, combined with the naturally occurring heat and humidity of summer in Alabama, presented a challenge to accurate data acquisition. An additional problem was that the recording computer was operated from a room about 100 feet from the cell, requiring a long cable to connect it to the signal sources.

The equipment for data collection is shown in the block diagrams in Figures 2.3a and 2.3b. The equipment included an IBM AT and an Analog Devices RTI-860 data acquisition board with Analog Devices 3B40-00 and 3B41-00 insolation amplifiers (the same as used in the laboratory cell tests). HEM Data Corporation Snapshot Storage Scope software was used to collect, display, and store the data. Inputs to the signal conditioning modules were available over sixteen (16) channels. Fourteen (14) channels were actually used. Six (6) of the channels were used to collect voltages across each of the six cermet anodes (voltage drop between the top of each anode stem and the cathode

---

(a) The sequence for exchanging anodes and the operating conditions of each of the anodes and the pilot cell as a whole will be discussed in a forthcoming report on the pilot cell test.

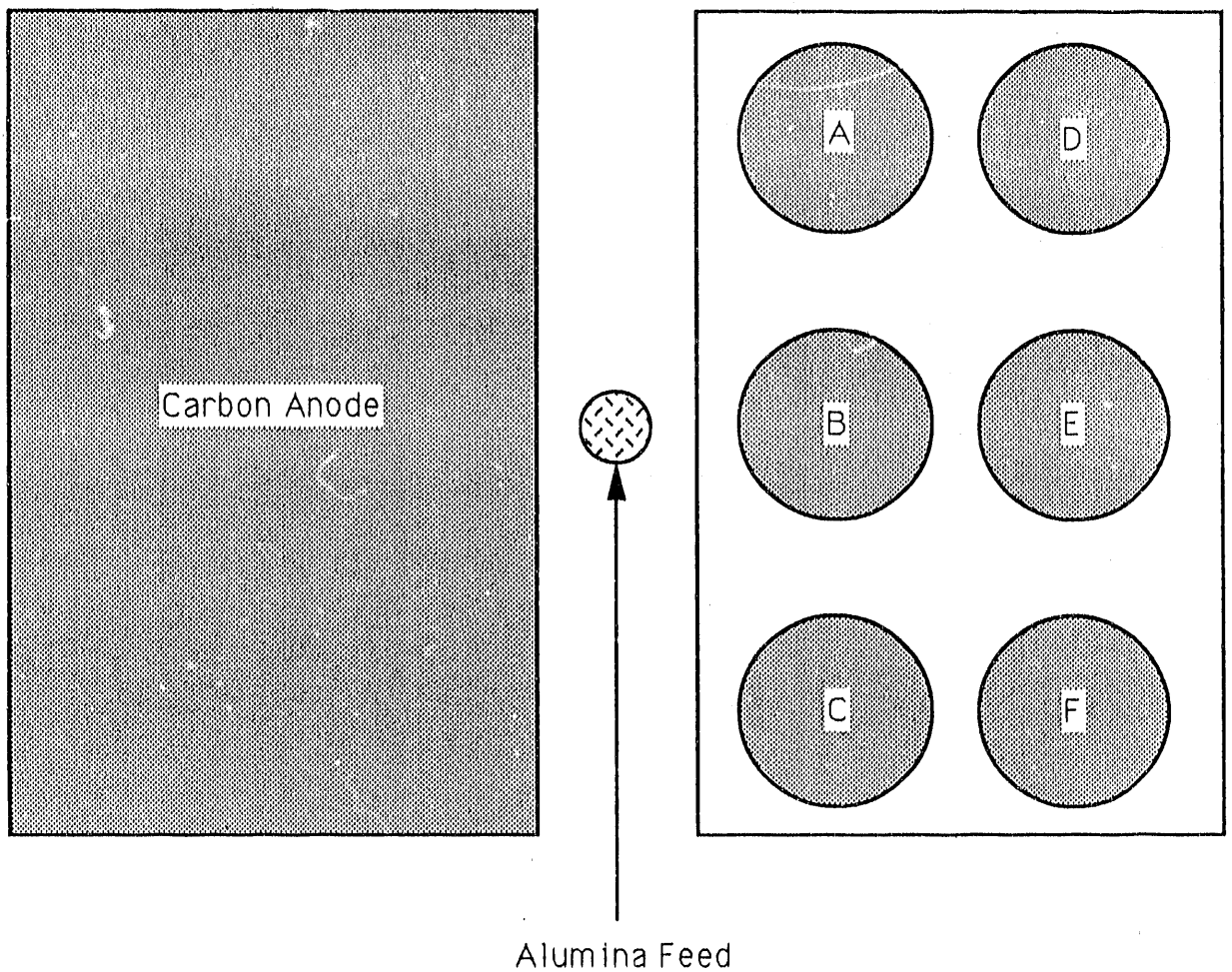

FIGURE 2.2. Arrangement of Anodes in the Pilot Cell Test

collector bar); six (6) were used for currents through each of the six cermet anodes (across 500 A: 100 mV shunts); and two (2) for the voltage and current through the large carbon anode.

The amplifiers had an isolated, floating input that allowed direct attachment to the voltage dividers and shunts on the pilot cell without concern for ground loops or common mode voltages. The nominal 0-10 kHz bandwidth of the amplifiers was reduced to 0-25 Hz (3 dB point) using plug-in filters. This bandwidth selection was based on previous experiments, which indicated that all useful sensor frequency data occurred below 25 Hz.

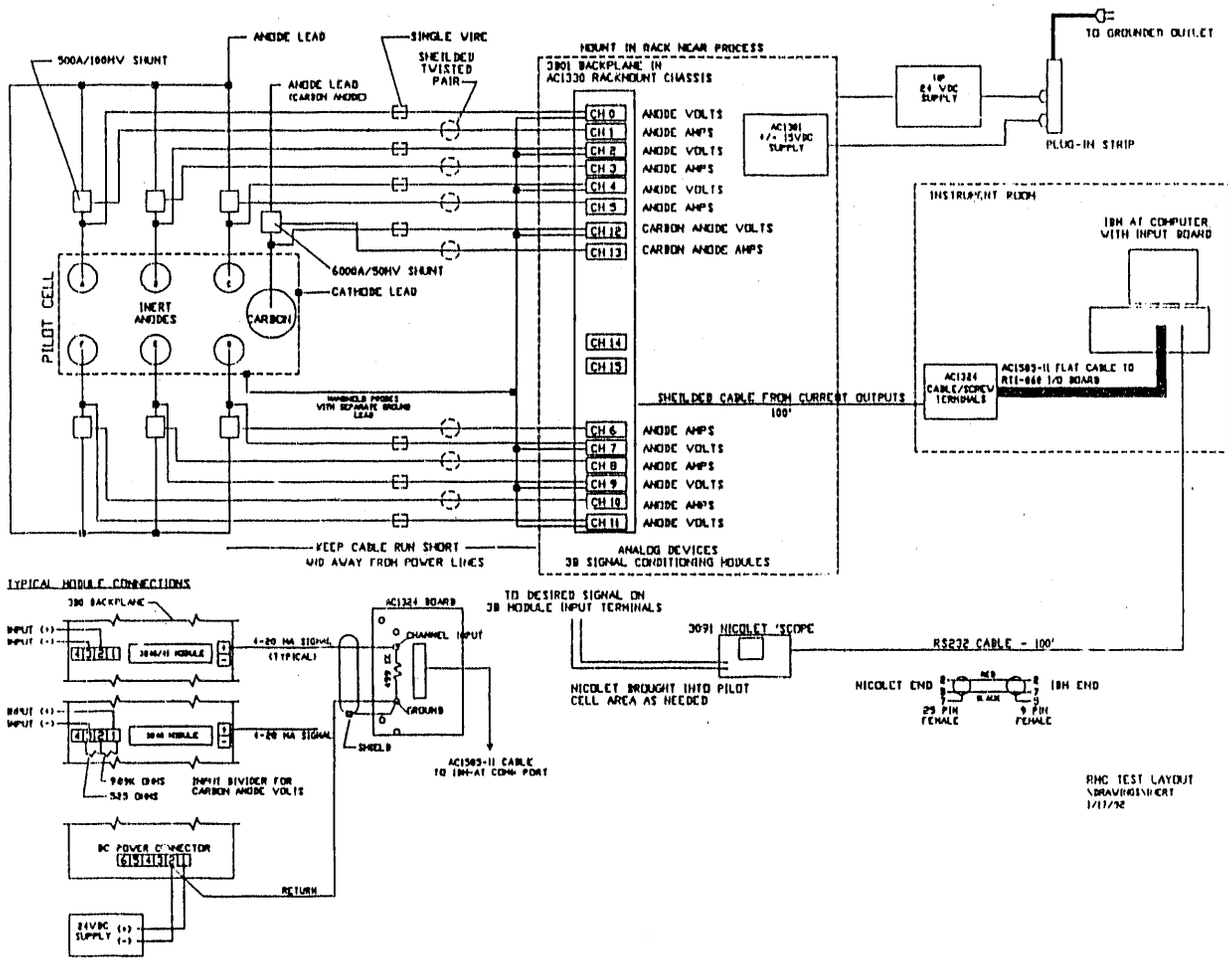

FIGURE 2.3a. Block Diagrams Showing Wiring of Data Acquisition System for the Pilot Cell Test

The output of the amplifiers was not isolated, nor was the input on the computer. The approximately 100 ft of cable run between the two units allowed both induced and common mode noise to cause problems. These problems were nearly eliminated by selecting the amplifier's current output rather than it's voltage output. Experimenting with combinations of the grounding location of the output cable shield and the AC power outlet used for the amplifiers eliminated the rest of the noise.

The current signal from the isolation amplifiers was changed to a voltage signal with a resistor mounted at the input to the analog data input board used in the computer. By making the conversion at the computer input, the

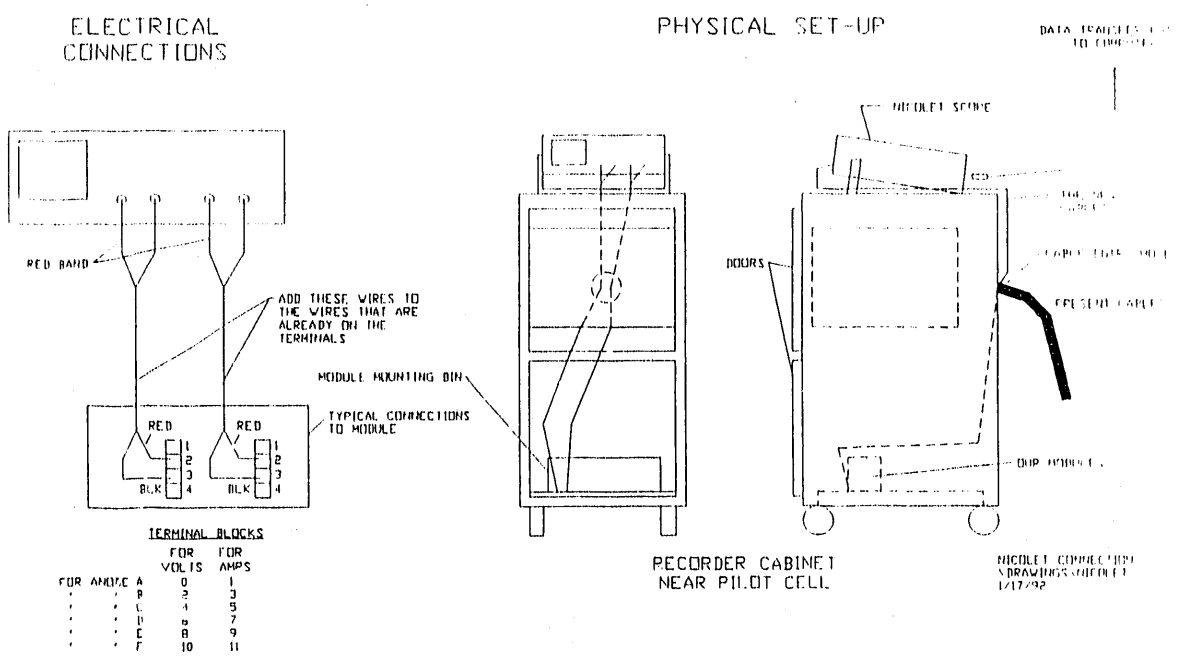

FIGURE 2.3b. Block Diagrams Showing Physical Setup of Data Acquisition System for the Pilot Cell Test

effect of any voltage drop or induced voltages along the 100 ft of cable was eliminated. This would not have been possible using a voltage signal from the amplifiers.

The DSA data were collected from the six cermet anodes and the carbon anode at 3 kHz sampling frequency over a period of 0.5 s (for a total of 1500 current and voltage measurements from each anode). The 3 kHz sampling frequency was sufficiently higher than the 25 Hz bandpass of the amplifiers to avoid "aliasing" effects but low enough to keep data files from exceeding the computer/software limitations. During each data acquisition period (about four times each day), three data files were collected in sequence. These sequential files were collected over a period of about 15 min and were regarded as "sampling in triplicate." Determining whether each of the three sequential files were similar enough to be regarded as triplicate measurements or whether significant variation of conditions occurred over the 15-min sampling period was one of the objectives of the data analysis. Clearly, if these files varied significantly from each other, the whole DSA approach would

be suspect since the objective was to correlate the signals to alumina concentration, which was sampled and measured over a much longer period (every 2 to 4 h).

Between August 10 and August 27, the cermet anodes were operated under "normal" conditions, i.e., at ≤ 90 A through each anode and with alumina concentration as close to saturation (about 8 wt%) as possible. Current and voltage data were collected routinely during this time and samples of bath were also collect for alumina concentration measurement. On August 27, alumina feed was stopped and the amount of alumina in the bath dropped. Data for DSA analysis and alumina concentration data were collected during this time also.

Other operating conditions for the pilot cell test were summarized in Windisch et al. (1991). Analysis of other data from the pilot cell test are not yet completed[(a)] but indicate numerous other variations of operating conditions with time (other than alumina concentration) that may have affected the results of this signal analysis study. Significant variations in anode currents, anode-to-cathode distance (ACD), the depth of anode immersion, current and potential on the carbon anode and on other inert anodes, and bath properties due to ledge formation and mucking occurred during the test. The characteristics of the cermet anodes themselves also changed due to corrosion.

Figure 2.4 shows the variation in alumina concentration, expressed as a percent of saturation (calculated from measured weight percentages using the formula by E. Skybakmoen, et al. 1990). As an example of fluctuations in other cell conditions, Figures 2.5 through 2.10 show the variation of current through each of the cermet anodes as a function of time during the pilot cell test. Table 2.1 summarizes all of the files collected for DSA analysis. The table indicates when these files were collected and lists some of the important operating conditions (such as when anodes were exchanged or when the "six-pack cluster" contained less than six cermet anodes). In plotting the

---

(a) Complete results of the pilot cell test operation and cermet anode performance will be discussed in a separate PNL report.

DSA data and alumina concentration data, time is referenced to "0 days" which is taken as 8/3/91 at 1400 h. This is the time that the first bath sample was taken for analysis.

2.3 DSA METHODS

Various DSA techniques were used to analyze the current and voltage signals. These included conductance computation, current-voltage power ratio, coherence and bicoherence indices between current and voltage, power spectrum estimation of signals, and linear and nonlinear modeling between the current and voltage. A description of each of these approaches is given in the Appendix.

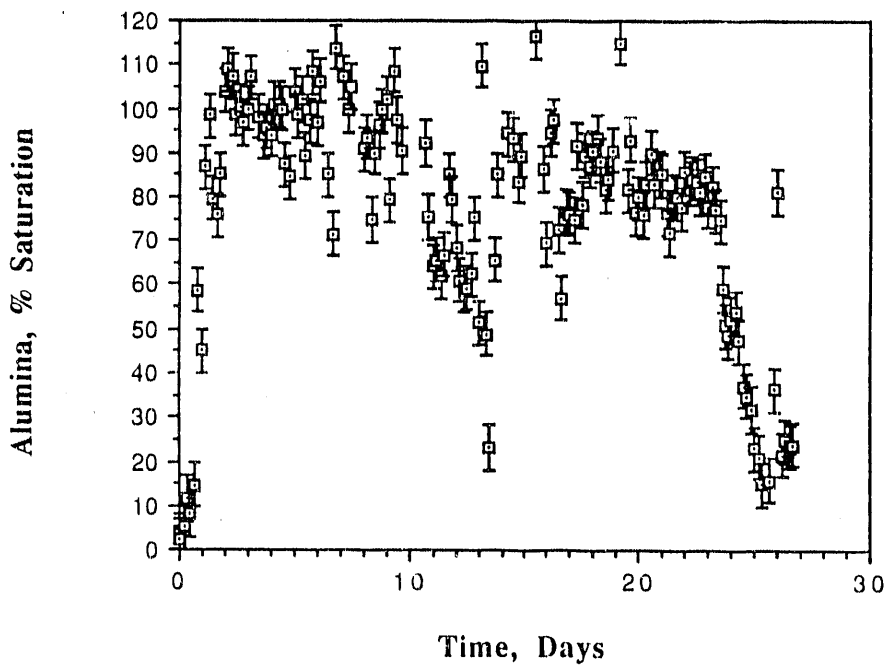

FIGURE 2.4. Variation of the Alumina Concentration with Time during the Pilot Cell Test. (Day = 0 corresponds to August 3, 1991, at 1400 h.)

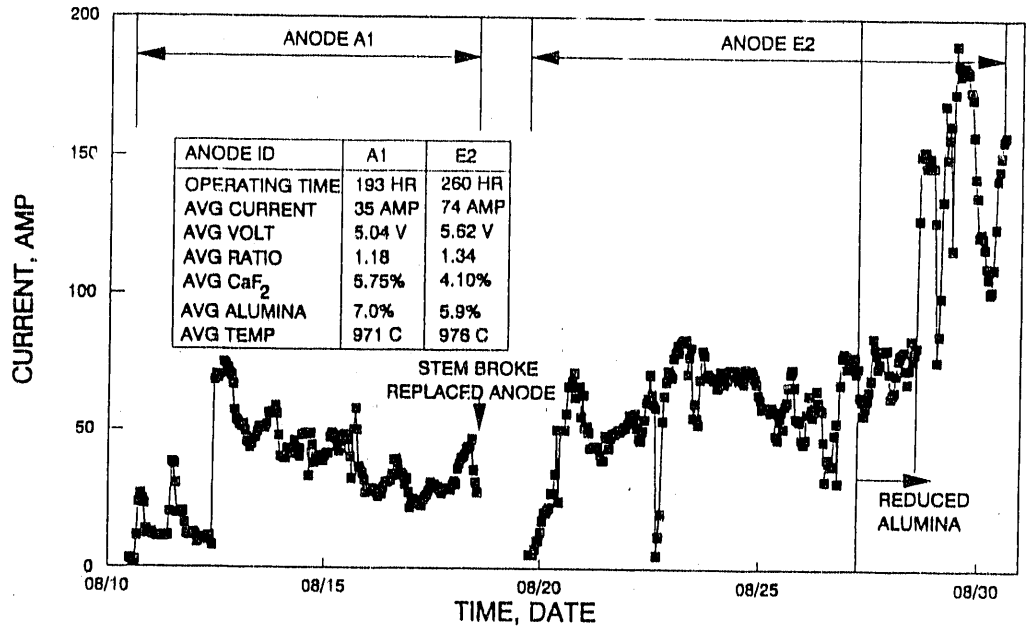

FIGURE 2.5. Variation in Current Through Anode in Position A during the Pilot Cell Test

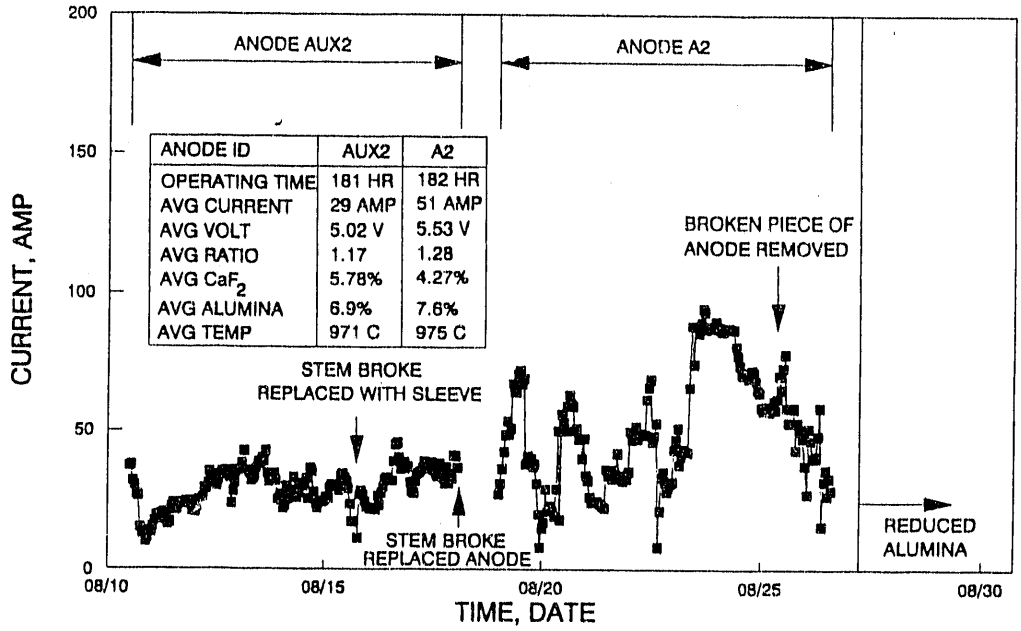

FIGURE 2.6. Variation in Current Through Anode in Position B during the Pilot Cell Test

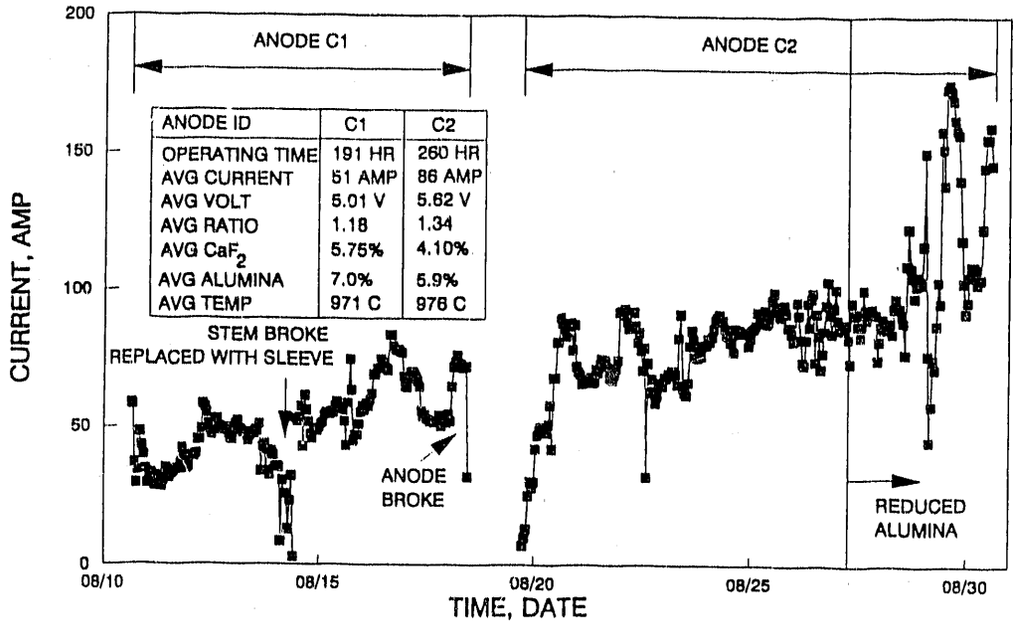

FIGURE 2.7. Variation in Current Through Anode in Position C during the Pilot Cell Test

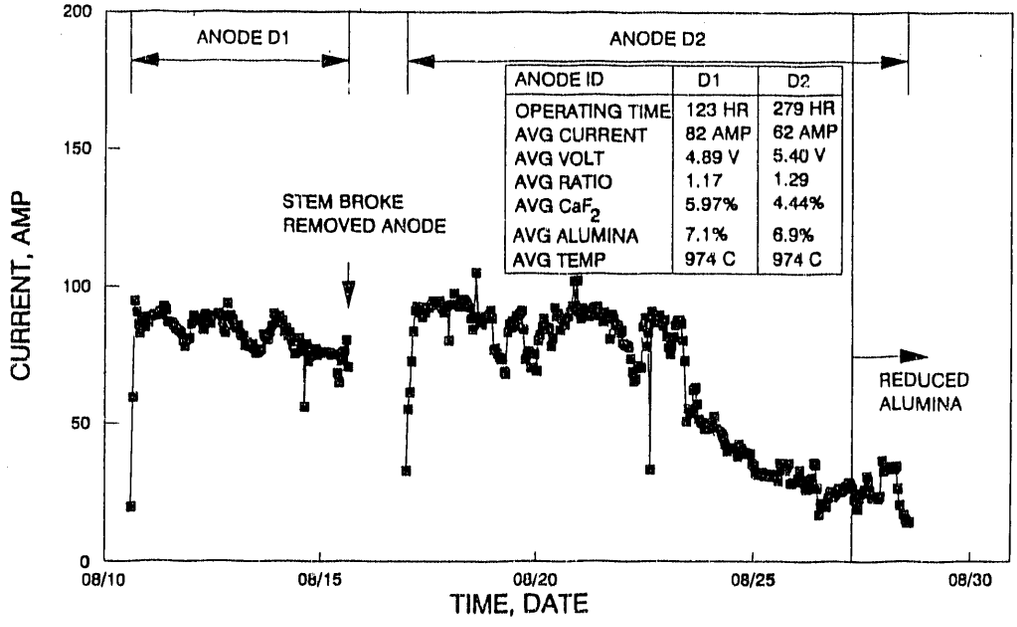

FIGURE 2.8. Variation in Current Through Anode in Position D during the Pilot Cell Test

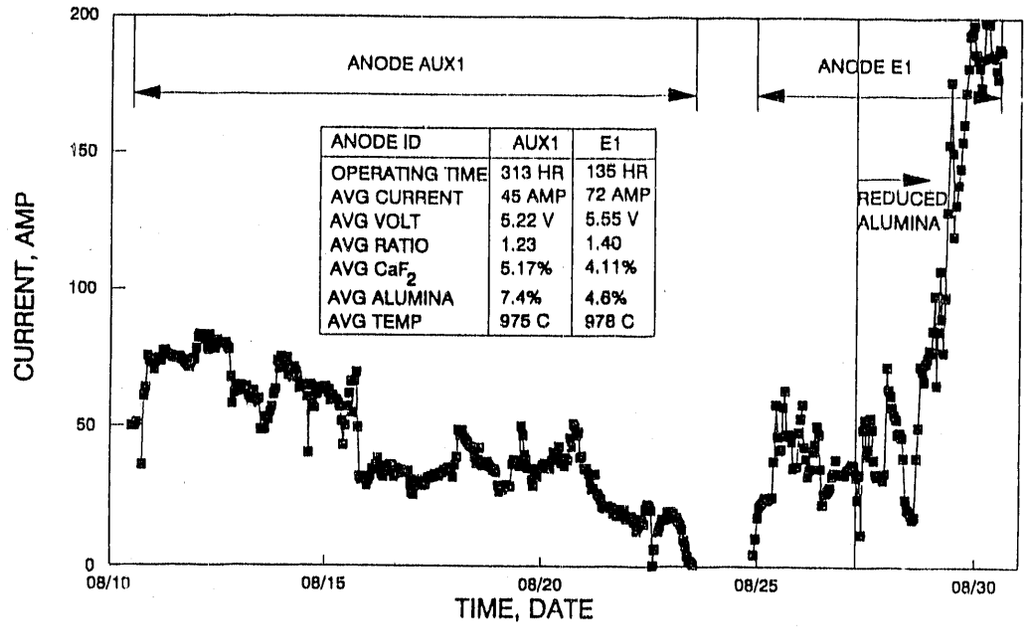

FIGURE 2.9. Variation in Current Through Anode in Position E during the Pilot Cell Test

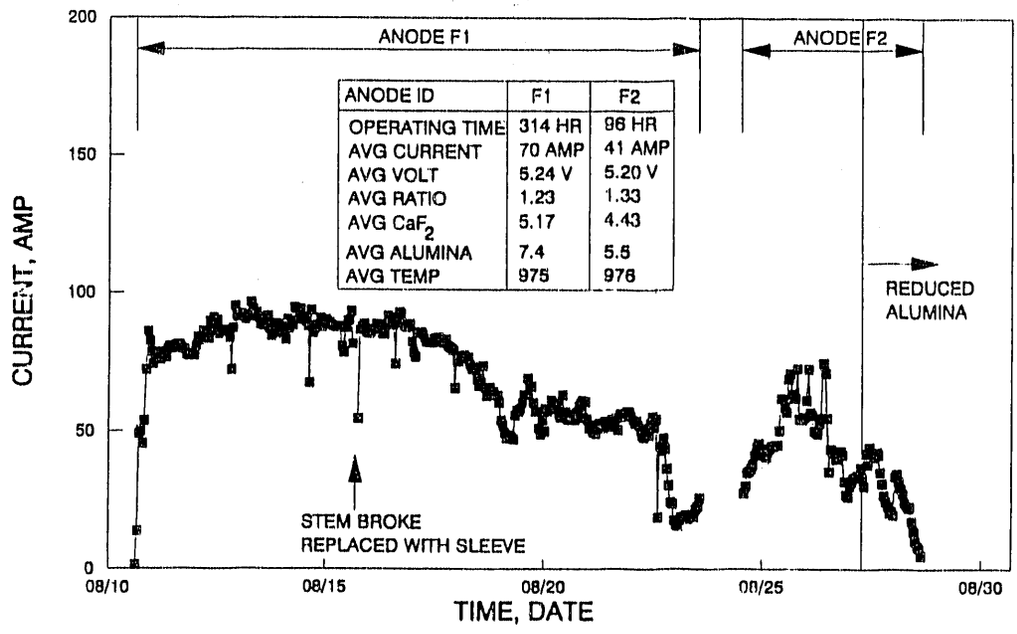

FIGURE 2.10. Variation in Current Through Anode in Position F during the Pilot Cell Test

TABLE 2.1. Pilot Cell Test DSA Data Files

	A	B	C	D	E	F	G
1	DATE	DATE (NUMBER)	TIME (HOURS)	TIME (DAYS)	DISK NAME	FILE NAME	COMMENT
2							
3	8/7/91	31995	1755	4.1479167	PC1	PC1A	Small carbon anodes in
4	8/7/91	31995	1800	4.1666667		PC1B	place of cermet anodes.
5	8/7/91	31995	1804	4.1683333		PC1C	
6	8/10/91	31998	1657	7.1070833	PC2	PC2A	Inert anodes all in.
7	8/10/91	31998	1702	7.1258333		PC2B	
8	8/10/91	31998	1706	7.1275		PC2C	
9	8/11/91	31999	742	7.7258333	PC3	PC3A	
10	8/11/91	31999	753	7.7304167		PC3B	
11	8/11/91	31999	806	7.7525		PC3C	
12	8/11/91	31999	2014	8.2558333	PC4	PC4A	
13	8/11/91	31999	2021	8.25875		PC4B	
14	8/11/91	31999	2025	8.2604167		PC4C	
15	8/12/91	32000	903	8.7929167	PC5	PC5A	
16	8/12/91	32000	910	8.7958333		PC5B	
17	8/12/91	32000	915	8.7979167		PC5C	
18	8/12/91	32000	1400	9	PC6	PC6A	
19	8/12/91	32000	1410	9.0041667		PC6B	
20	8/12/91	32000	1415	9.00625		PC6C	
21	8/12/91	32000	1732	9.1383333	PC7	PC7A	
22	8/12/91	32000	1745	9.14375		PC7B	
23	8/12/91	32000	1751	9.14625		PC7C	
24	8/13/91	32001	810	9.7541667	PC8	PC8A	
25	8/13/91	32001	814	9.7558333		PC8B	
26	8/13/91	32001	818	9.7575		PC8C	
27	8/13/91	32001	1330	9.9708333	PC9	PC9A	
28	8/13/91	32001	1334	9.9725		PC9B	
29	8/13/91	32001	1338	9.9741667		PC9C	
30	8/13/91	32001	1630	10.095833	PC10	PC10A	
31	8/13/91	32001	1635	10.097917		PC10B	
32	8/13/91	32001	1639	10.099583		PC10C	
33	8/14/91	32002	912	10.796667	PC11	PC11A	
34	8/14/91	32002	918	10.799167		PC11B	
35	8/14/91	32002	954	10.814167		PC11C	
36	8/15/91	32003	925	11.802083	PC12	PC12A	
37	8/15/91	32003	930	11.804167		PC12B	
38	8/15/91	32003	935	11.80625		PC12C	
39	8/15/91	32003	1325	11.96875	PC13	PC13A	
40	8/15/91	32003	1332	11.971667		PC13B	
41	8/15/91	32003	1342	11.975833		PC13C	
42	8/15/91	32003	1610	12.0875	PC14	PC14A	Stubs on Anodes B, D and F
43	8/15/91	32003	1702	12.125833		PC14B	are broken.
44	8/15/91	32003	1708	12.128333		PC14C	
45	8/15/91	32003	2142	12.309167	PC15	PC15A	Anode D is out.
46	8/15/91	32003	2146	12.310833		PC15B	
47	8/15/91	32003	2150	12.3125		PC15C	
48	8/16/91	32004	904	12.793333	PC16	PC16A	
49	8/16/91	32004	909	12.795417		PC16B	
50	8/16/91	32004	916	12.798333		PC16C	
51	8/16/91	32004	1307	12.96125	PC17	PC17A	
52	8/16/91	32004	1312	12.963333		PC17B	

TABLE 2.1. (contd)

	A	B	C	D	E	F	G
53	8/16/91	32004	1317	12.965417		PC17C	
54	8/16/91	32004	1747	13.144583	PC18	PC18A	
55	8/16/91	32004	1752	13.146667		PC18B	
56	8/16/91	32004	1758	13.149167		PC18C	
57	8/16/91	32004	2143	13.309583	PC19	PC19A	
58	8/16/91	32004	2148	13.311667		PC19B	
59	8/16/91	32004	2156	13.315		PC19C	
60	8/17/91	32005	821	13.75875	PC20	PC20A	
61	8/17/91	32005	825	13.760417		PC20B	
62	8/17/91	32005	830	13.7625		PC20C	
63	8/17/91	32005	2134	14.305833	PC21	PC21A	
64	8/17/91	32005	2148	14.311667		PC21B	
65	8/17/91	32005	2152	14.313333		PC21C	
66	8/18/91	32006	942	14.809167	PC22	PC22A	Anode B is out.
67	8/18/91	32006	947	14.81125		PC22B	
68	8/18/91	32006	953	14.81375		PC22C	
69	8/18/91	32006	2018	15.2575	PC23	PC23A	Anodes A, B, and C are out.
70	8/18/91	32006	2023	15.259583		PC23B	
71	8/18/91	32006	2028	15.261667		PC23C	
72	8/19/91	32007	844	15.768333	PC24	PC24A	Anodes A and C are out.
73	8/19/91	32007	850	15.770833		PC24B	
74	8/19/91	32007	856	15.773333		PC24C	
75	8/19/91	32007	1255	15.939583	PC25	PC25A	Anodes A and C are out.
76	8/19/91	32007	1301	15.95875		PC25B	
77	8/19/91	32007	1307	15.96125		PC25C	
78	8/19/91	32007	1722	16.134167	PC26	PC26A	Anodes A and C are out.
79	8/19/91	32007	1726	16.135833		PC26B	
80	8/19/91	32007	1733	16.13875		PC26C	
81	8/19/91	32007	2213	16.33875	PC27	PC27A	All inert anodes are in.
82	8/19/91	32007	2218	16.340833		PC27B	
83	8/19/91	32007	2223	16.342917		PC27C	
84	8/20/91	32008	822	16.759167	PC28	PC28A	
85	8/20/91	32008	828	16.761667		PC28B	
86	8/20/91	32008	833	16.76375		PC28C	
87	8/20/91	32008	1300	16.958333	PC29	PC29A	
88	8/20/91	32008	1305	16.960417		PC29B	
89	8/20/91	32008	1310	16.9625		PC29C	
90	8/20/91	32008	1605	17.085417	PC30	PC30A	
91	8/20/91	32008	1609	17.087083		PC30B	
92	8/20/91	32008	1617	17.090417		PC30C	
93	8/20/91	32008	2212	17.338333	PC31	PC31A	
94	8/20/91	32008	2222	17.3425		PC31B	
95	8/20/91	32008	2228	17.345		PC31C	
96	8/21/91	32009	823	17.759583	PC32	PC32A	
97	8/21/91	32009	828	17.761667		PC32B	
98	8/21/91	32009	833	17.76375		PC32C	
99	8/21/91	32009	1337	17.97375	PC33	PC33A	
100	8/21/91	32009	1345	17.977083		PC33B	
101	8/21/91	32009	1349	17.97875		PC33C	
102	8/21/91	32009	1550	18.0625	PC34	PC34A	
103	8/21/91	32009	1610	18.0875		PC34B	
104	8/21/91	32009	1616	18.09		PC34C	

TABLE 2.1. (contd)

	A	B	C	D	E	F	G
105	8/21/91	32009	2210	18.3375	PC35	PC35A	
106	8/21/91	32009	2214	18.339167		PC35B	
107	8/21/91	32009	2218	18.340833		PC35C	
108	8/22/91	32010	800	18.75	PC36	PC36A	
109	8/22/91	32010	806	18.7525		PC36B	
110	8/22/91	32010	811	18.754583		PC36C	
111	8/22/91	32010	1605	19.085417	PC37	PC37A	Carbon anodes was just
112	8/22/91	32010	1612	19.088333		PC37B	replaced. Volts are high.
113	8/22/91	32010	1618	19.090833		PC37C	
114	8/23/91	32011	840	19.766667	PC38	PC38A	Currents on Anodes E and F
115	8/23/91	32011	843	19.767917		PC38B	are low.
116	8/23/91	32011	847	19.769583		PC38C	
117	8/23/91	32011	1105	19.877083	PC39	PC39A	
118	8/23/91	32011	1109	19.87875		PC39B	
119	8/23/91	32011	1118	19.8825		PC39C	
120	8/23/91	32011	1640	20.1	PC40	PC40A	Anodes E and F are out.
121	8/23/91	32011	1646	20.1025		PC40B	
122	8/23/91	32011	1651	20.104583		PC40C	
123	8/24/91	32012	925	20.802083	PC41	PC41A	Anodes E and F are out.
124	8/24/91	32012	932	20.805		PC41B	
125	8/24/91	32012	938	20.8075		PC41C	
126	8/24/91	32012	1334	20.9725	PC42	PC42A	All anodes are in, but no
127	8/24/91	32012	1340	20.975		PC42B	current on Anode E.
128	8/24/91	32012	1346	20.9775		PC42C	
129	8/24/91	32012	1604	21.085	PC43	PC43A	No current on Anode E.
130	8/24/91	32012	1609	21.087083		PC43B	
131	8/24/91	32012	1614	21.089167		PC43C	
132	8/25/91	32013	717	21.715417	PC44	PC44A	All inert anodes are in and
133	8/25/91	32013	722	21.7175		PC44B	carrying current.
134	8/25/91	32013	726	21.719167		PC44C	
135	8/25/91	32013	1529	22.05375	PC45	PC45A	
136	8/25/91	32013	1535	22.05625		PC45B	
137	8/25/91	32013	1539	22.057917		PC45C	
138	8/25/91	32013	1546	22.060833	PC46	PC46A	
139	8/25/91	32013	1552	22.063333		PC46B	
140	8/25/91	32013	1556	22.065		PC46C	
141	8/26/91	32014	852	22.771667	PC47	PC47A	
142	8/26/91	32014	856	22.773333		PC47B	
143	8/26/91	32014	860	22.775		PC47C	
144	8/26/91	32014	924	22.801667	PC48	PC48A	
145	8/26/91	32014	929	22.80375		PC48B	
146	8/26/91	32014	934	22.805833		PC48C	
147	8/26/91	32014	939	22.807917	PC49	PC49A	
148	8/26/91	32014	945	22.810417		PC49B	
149	8/26/91	32014	949	22.812083		PC49C	
150	8/26/91	32014	1646	23.1025	PC50	PC50A	Anode B is out for rest of
151	8/26/91	32014	1654	23.105833		PC50B	test.
152	8/26/91	32014	1658	23.1075		PC50C	
153	8/26/91	32014	1704	23.126667	PC51	PC51A	
154	8/26/91	32014	1709	23.12875		PC51B	
155	8/26/91	32014	1714	23.130833		PC51C	
156	8/27/91	32015	804	23.751667	PC52	PC52A	Alumina feed stopped.

TABLE 2.1. (contd)

	A	B	C	D	E	F	G
157	8/27/91	32015	810	23.754167		PC52B	
158	8/27/91	32015	815	23.75625		PC52C	
159	8/27/91	32015	826	23.760833	PC53	PC53A	
160	8/27/91	32015	833	23.76375		PC53B	
161	8/27/91	32015	838	23.765833		PC53C	
162	8/27/91	32015	1020	23.841667	PC54	PC54A	
163	8/27/91	32015	1027	23.844583		PC54B	
164	8/27/91	32015	1032	23.846667		PC54C	
165	8/27/91	32015	1158	23.899167	PC55	PC55A	
166	8/27/91	32015	1204	23.918333		PC55B	
167	8/27/91	32015	1209	23.920417		PC55C	
168	8/27/91	32015	1356	23.981667	PC56	PC56A	
169	8/27/91	32015	1401	24.000417		PC56B	
170	8/27/91	32015	1405	24.002083		PC56C	
171	8/27/91	32015	1541	24.05875	PC57	PC57A	
172	8/27/91	32015	1546	24.060833		PC57B	
173	8/27/91	32015	1550	24.0625		PC57C	
174	8/27/91	32015	1937	24.22375	PC58	PC58A	
175	8/27/91	32015	1942	24.225833		PC58B	
176	8/27/91	32015	1947	24.227917		PC58C	
177	8/28/91	32016	826	24.760833	PC59	PC59A	
178	8/28/91	32016	832	24.763333		PC59B	
179	8/28/91	32016	837	24.765417		PC59C	
180	8/28/91	32016	1048	24.853333	PC60	PC60A	
181	8/28/91	32016	1101	24.875417		PC60B	
182	8/28/91	32016	1106	24.8775		PC60C	
183	8/28/91	32016	1305	24.960417	PC61	PC61A	
184	8/28/91	32016	1311	24.962917		PC61B	
185	8/28/91	32016	1315	24.964583		PC61C	

3.0 RESULTS OF ANALYSIS

There were a very large number of relationships evaluated in this work between the various quantification parameters selected for analysis (derived from the current and voltage signals) and alumina concentration. The relationships were first tested on the data collected from the laboratory cells at PNL. Some conclusions were then drawn regarding parameters that appeared to show the "best" correlation with alumina concentration. These (most promising) parameters were then applied to the pilot cell data to determine the effects of scale-up.

3.1 LABORATORY CELL TESTS

Laboratory cell tests were conducted at PNL to provide data for evaluating the sensitivity of quantification parameters to alumina concentration, current density, signal frequency, and ACD.

3.1.1 Variations with Alumina Concentration

The laboratory cell data were used to screen a very large number of quantification parameters (calculated from the current and voltage signals) for those that showed the most promising correlation with alumina concentration. (See the Appendix for a description of some of these parameters.)

The earliest data collected from the laboratory cells, i.e., those labelled "ACD data" and "DSA data" (corresponding to "ACD tests" and "DSA tests" discussed in the Procedures Section), appeared to show a correlation between three quantification parameters and alumina concentration. These parameters were 1) the conductance,[a] L, 2) the second filter coefficient, COEF2, and 3) the sixth filter coefficient, COEF6, of the linear modeling method. (See Appendix for definition of these parameters.) Success with using L was considered consistent with the similar, although more limited, information obtained with the total power functions for current and voltage,

---

(a) Conductance values are normalized so their units are not those normally used for conductance. In any event, only relative values and their variations were important in this study.

separately, that was discussed in Windisch et al. (1990). Later analysis using laboratory data labelled "Set#3 data" and the pilot cell data reduced some of the initial optimism regarding reproducible application of these three parameters to monitor alumina concentration. In particular, the parameters and their apparent correlations with alumina appeared either to be overly sensitive to other cell operating conditions or were simply not as sensitive to alumina concentration as was previously thought from the results of analyzing the earlier data sets.

Plots of L, COEF2, and COEF6 versus alumina concentration for the ACD and DSA data are shown in Figures 3.1, 3.2, and 3.3, respectively. Data are presented in each plot for different current densities, with ACD = 1.5 in., and with a superimposed ripple of ±10 mV or ±50 mV at 10 Hz. (The ripple is required for calculation of COEF2 and COEF6.) Similar results were obtained for other ACD values, both with and without the applied AC ripple.

In each case the curves are relatively "flat" at lower current densities and have a slight positive slope at higher current densities.[a] There is also a slight dip in the curves at alumina concentrations between 4 and 6 wt%. This dip was observed in most of the data. Generally, the dip was more distinct for the ±10 mV data (ACD tests) than for the ±50 mV data (DSA tests). At concentrations above 6 wt%, the data appear noisier, as in the cases of COEF2 and COEF6, or are very flat, as in the case of L.

Considering all aspects of the ACD and DSA data, it was still unclear if a relationship suitable for an alumina sensor was achievable. The above results appeared promising, but there appeared to be important deficiencies. The strongest dependency (largest slope) between the parameters and alumina concentration was in the vicinity of the dip between 4 and 6 wt%. However, it was not clear whether the dip was reproducible. Different data, albeit collected with different AC excitation voltages, gave dips with somewhat different appearances. There was a question also as to whether there was any

---

(a) It is not clear why the conductance increases with alumina concentration in these plots. Conductance should decrease as discussed in numerous references (Grjotheim et al. 1982).

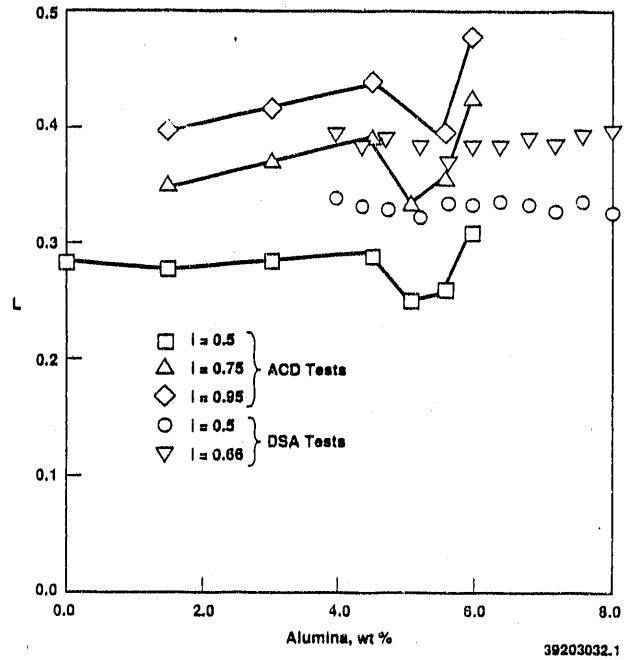

FIGURE 3.1. Plot of Conductance, L, by Cross-Correlation versus Weight Percent Alumina at Various Current Densities. (ACD = 1.5 in.; a 10 Hz Ripple was Used.)

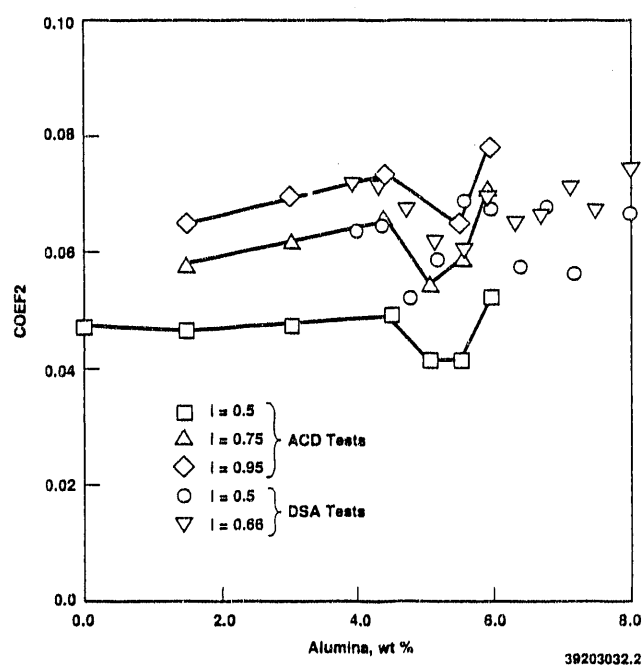

FIGURE 3.2. Plot of COEF2 versus Weight Percent Alumina at Various Current Densities. (ACD = 1.5 in.; a 10 Hz Ripple was Used.)

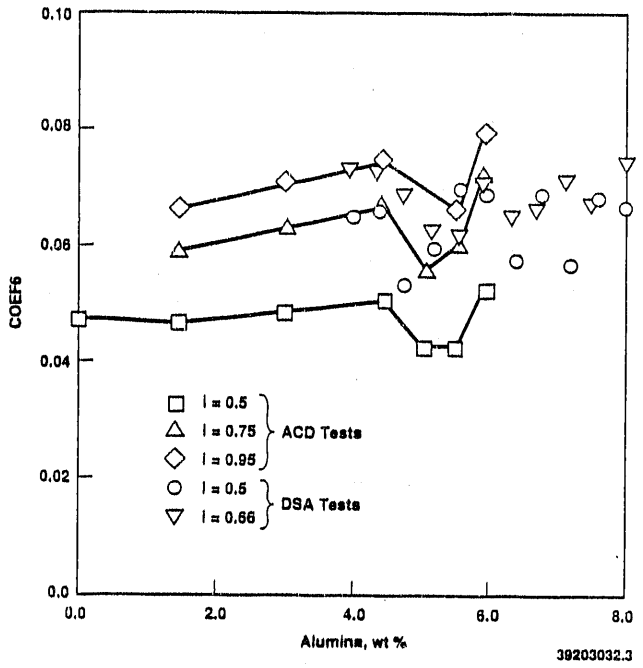

FIGURE 3.3. Plot of COEF6 versus Weight Percent Alumina at Various Current Densities. (ACD = 1.5 in.; a 10 Hz Ripple was Used.)

dependence on the size of the AC ripple. Sensitivity to the ripple would suggest a problem in applying this technology to commercial cells. The idea was to use noise inherent in the commercial cell rectifiers as the ripple. Ordinarily this noise can be expected to vary appreciably during cell operation. Sensitivity of the quantification parameter to this variation would make the above approach unreliable. Finally, since the primary objective of this work was a parameter showing sensitivity to high alumina concentrations, sensitivity only in the intermediate ranges, i.e., 4 to 6 wt% where 8 wt% is saturation, would appear to be a disadvantage.

To address the above concerns, a followup data set (Set#3) was collected using the laboratory cells. Specifically, these experiments were meant to 1) determine the general reproducibility of the results from the ACD and DSA data, 2) see if the "dip" between 4 and 6 wt% could be reproduced and to quantify it better, and 3) obtain more data in the 6 to 8 wt% range where alumina sensitivity is especially important.

Unfortunately, the Set#3 data gave varied behavior which could not corroborate the results from the earlier data. For example, as shown in Figure 3.4, a "dip" was observed in L, COEF2, and COEF6 when the current density was 0.75 A/cm^2--but it occurred at 3 wt% alumina instead of in the expected 4 to 6 wt% range.[a] More importantly, as also shown in Figure 3.4, there was no significant and consistent correlation with alumina concentration at higher weight percent values. This result was especially disappointing since the need for sensitivity at higher concentrations was a prerequisite for a sensor to be used successfully with the cermet anodes.

3.1.2 Variations with Current Density

In addition to screening for sensitivity to alumina concentration, the quantification parameters were tested for sensitivity to other operating conditions including current density. COEF2 and COEF6 both exhibited maxima in most cases at current densities close to 0.5 A/cm^2. This is illustrated by Figure 3.5 which shows the variation of COEF2 with current density at various alumina concentrations for cells with ACD = 3.0 in. and with a superimposed ripple of ±10 mV at 10 Hz. Similar results were observed for other ACD values and types of ripples. The result is consistent with impedance measurements made at PNL and DSA results for resistance reported in FY 1989 that showed an impedance or resistance minimum near 0.5 A/cm^2. The relationship appears to be particularly strong in the case of COEF2 and COEF6. The interesting thing about the more recent data is that COEF2 and COEF6 are obtained from a linear model for conductance that includes the effect of "memory." Each conductance value is calculated by reference to previous data points, i.e., in the time domain. The parameters therefore take on the properties of capacitance. These results suggest that including the capacitive effects may improve the sensitivity of the conductance or resistance parameters. Consequently, the parameters COEF2 and COEF6 were considered appropriate in the search for a

---

(a) There is also a possibility that the single point contributing to this difference may have been a "flier." In light of the atypical behavior of this one point (compared to the other data in Figure 3.4), it is recommended that not too much significance be placed on this dip until replicate data are obtained.

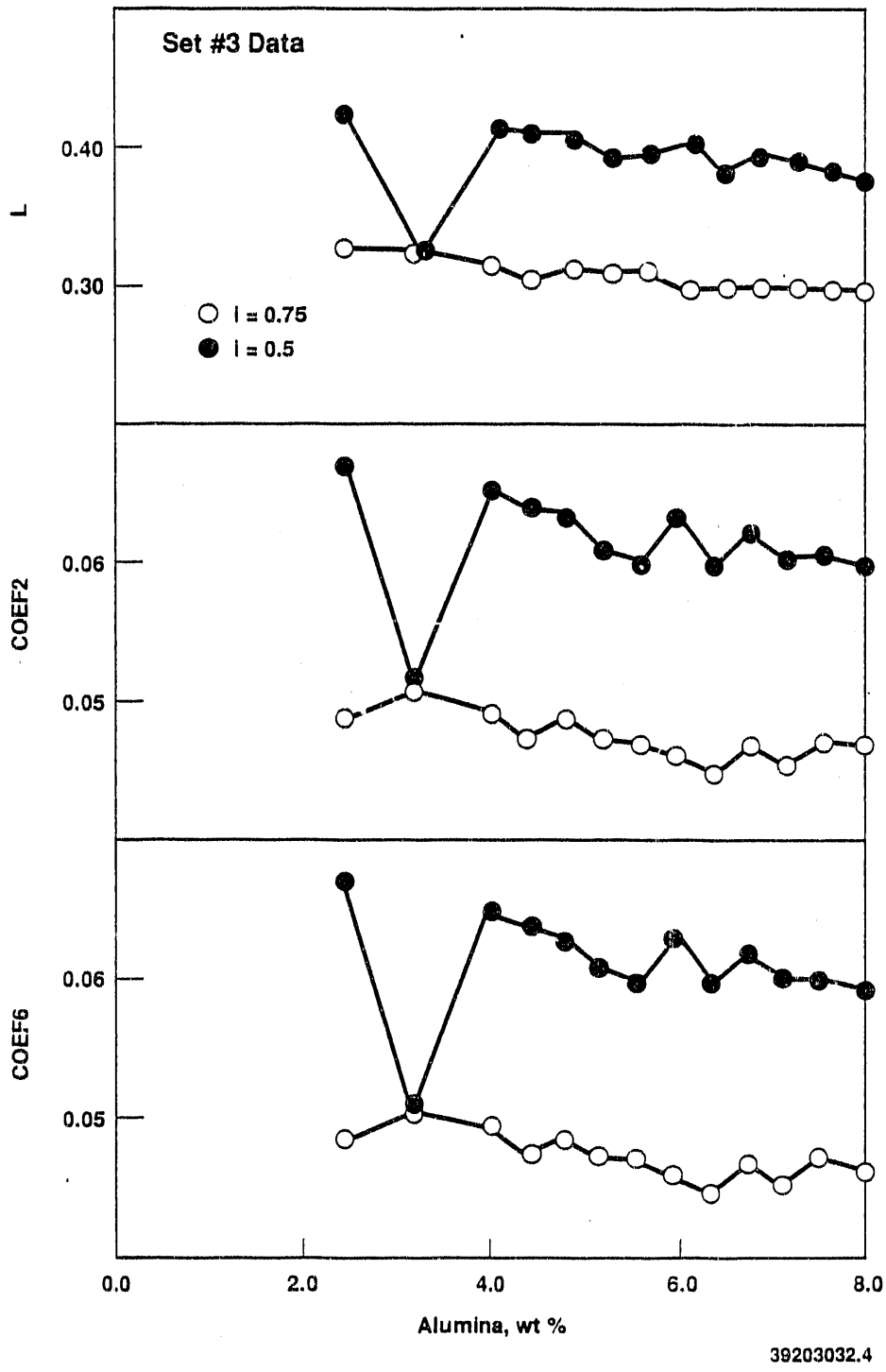

FIGURE 3.4. Plots of L, COEF2 and COEF6 versus Weight Percent Alumina for Set#3 Data. (ACD = 1.5 in.; a 10 Hz Ripple was Used.)

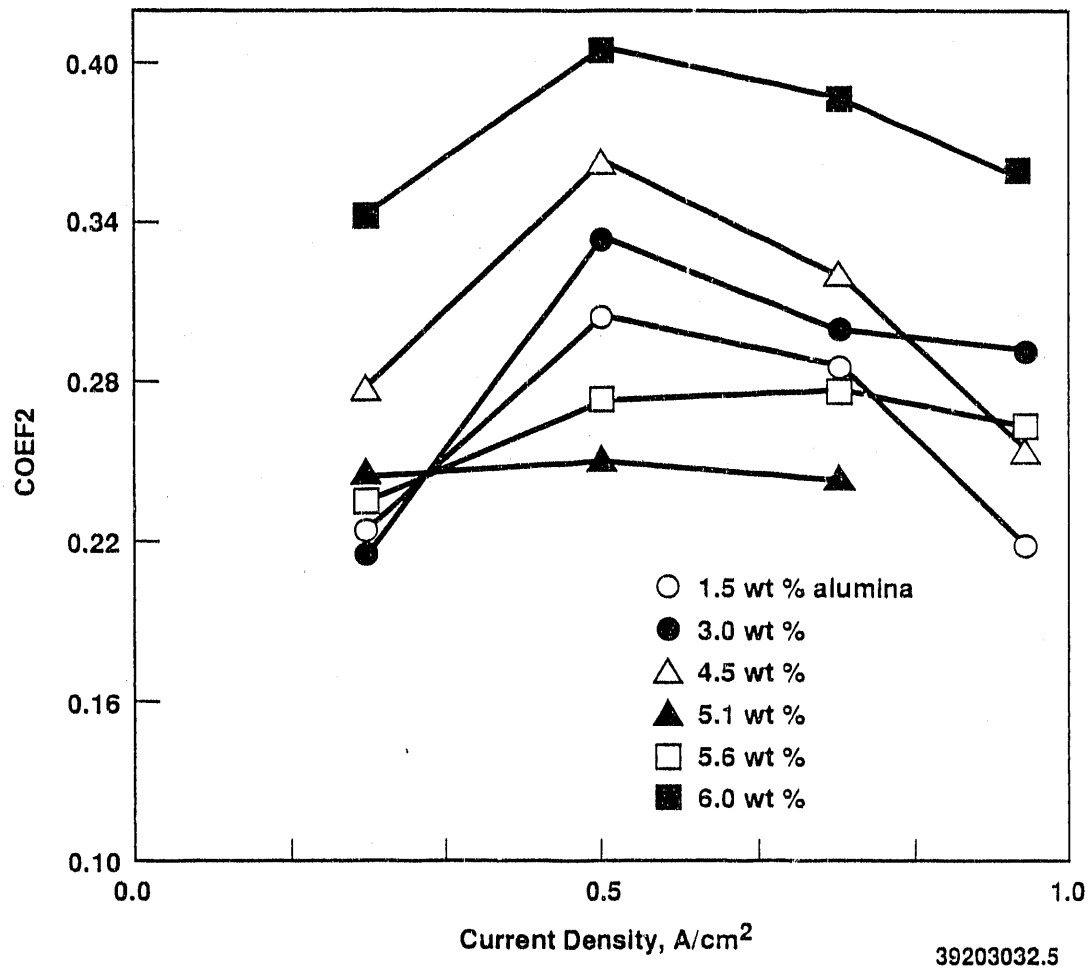

FIGURE 3.5. Plot of COEF2 versus Current Density for Various Alumina Concentrations. (ACD = 3.0; a 10 Hz Ripple was Used.)

sensitive parameter/alumina correlation. This is why these two parameters were selected for further study in both the laboratory cell tests and the pilot cell test.

3.1.3 The Frequency Spectrum and Sensitivity

Plots in this work were generated using voltage and current signals having a frequency content between 0 and 10 kHz. In addition, plots were generated with voltage and current signals low-passed at a cutoff frequency of 25 Hz (very low frequency content). These two types of plots are compared in Figure 3.6. As shown, the results are essentially identical. This same

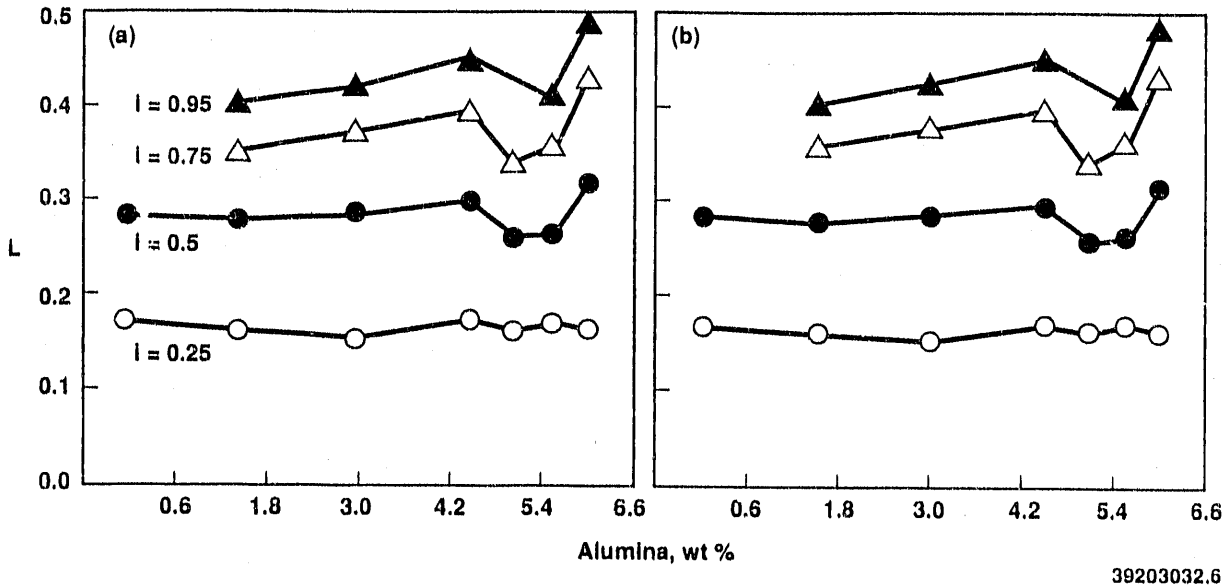

FIGURE 3.6. Comparison of Conductance versus Weight Percent Alumina Data a) With and b) Without a 25 Hz Low-Pass Filter

comparison was obtained for nearly all of the laboratory-scale data sets in this work. Consequently, it appeared that the quantification parameters under study depended only on the low frequency content of the signals. There appeared to be no empirically based reason to pursue the collection of signals with frequencies higher than those studied in the laboratory tests or the analysis of signals with frequencies greater than 25 Hz.

The results of another experiment reinforce the above conclusions. Digital voltage and current signals were collected from a 2-ohm resistor connected to the instrumentation in place of the laboratory cell. Much of the noise in this test, all of which was attributed to instrumentation, occurred at higher frequencies, above 25 Hz. Consequently, by low-passing the voltage and current signals, not only do we retain all of the important process-related information, but we also reject most of the instrumental noise. Based on these results, low-pass filters were used in the pilot cell test reported in Section 3.2.

3.1.4 Variations with ACD

Another approach that was tested in FY 1990 was to determine whether any correlations existed between second order relationships involving cell operating conditions and the various quantification parameters. If successful, these second order relationships could be determined online with only slightly more difficulty than the direct measurements discussed above.

The second order relationship tested in this work was the derivative of the slope of the resistance-versus-ACD response with respect to the alumina concentration. Ignoring impedance terms associated with the electrode processes, the aluminum reduction cell can be viewed as a simple conductance cell whose resistance is simply the resistance of the electrolyte.[a] If R is the electrolyte resistance, K is the cell constant, and ρ is the resistivity of the electrolyte, then

$$R = K\rho \tag{3.1}$$

Taking the derivative with respect to the ACD, gives

$$dR/d(ACD) = K[d\rho/d(ACD)] + \rho[dK/d(ACD)] \tag{3.2}$$

ρ, of course, should not depend on the ACD, so

$$dR/d(ACD) = C\rho \tag{3.3}$$

(a) This assumption is good only at low cell currents. At higher currents contributions from the resistances of the electrodes, leads, and collector bars must also be considered. There is also a contribution from bubble resistance which is formally neglected in this approach, but may also be considered as part of the electrolyte impedance.

where C = dK/d(ACD) is a constant and dependent on the cell geometry.[a]

Taking the derivative of Equation 3.3 with respect to the alumina concentration, A, gives

$$d[dR/d(ACD]/dA = C(d\rho/dA) \tag{3.4}$$

In these DSA-based approaches, some of the quantification parameters are related directly to the cell resistance, so we can replace R with the generic quantification parameter, X, and a new constant, C′, to preserve dimensionality.

$$d[dX/d(ACD)]/dA = C'(d\rho/dA) \tag{3.5}$$

Since ρ and dρ/dA are both nonzero and functions of alumina concentration, dX/d(ACD) should be a function of alumina concentration also and may therefore be useful as the basis for an alumina sensor. The approach was conceived of as an alternative to the first order relationship between X and A. If X is not sensitive enough to A, perhaps dX/d(ACD) will be.

If dX/d(ACD) showed a significant dependency on alumina concentration, using it would be relatively straightforward. An operator would need to vary the ACD while collecting DSA data. A computer would calculate X from the digital data, and, subsequently, determine dX/d(ACD). With a calibration curve developed for the cell, dX/d(ACD) could then be related to the alumina concentration. The principal issue to be addressed in this preliminary work, however, is whether dX/d(ACD) is sensitive enough to alumina concentration to serve as the basis of a practical alumina sensor.

(a) This assumes linearity, which may not be the case. The assumption is made as a first approximation only. Fanning currents may impart severe departure from linear behavior, particularly at large ACD values. Alternatively, the approximation may not be as severe at the smaller ACD values tested (0.75 and 1.5 in.).

Digital signal data were collected from laboratory cells with ACD values equal to 0.75, 1.5, 2.25, and 3.0 in. At each of these ACD values, data were collected for various alumina concentrations, and also at various anode potentials/current densities. AC ripple tests were also performed as discussed previously. In all cases, the various quantification parameters derived from the DSA data showed no significant and reproducible variation with ACD. For example, Figure 3.7 shows a plot of the conductance estimated by cross-correlation (the reciprocal of resistance or impedance), L, as a function of ACD at a current density of 0.75 A/cm^2 and various alumina

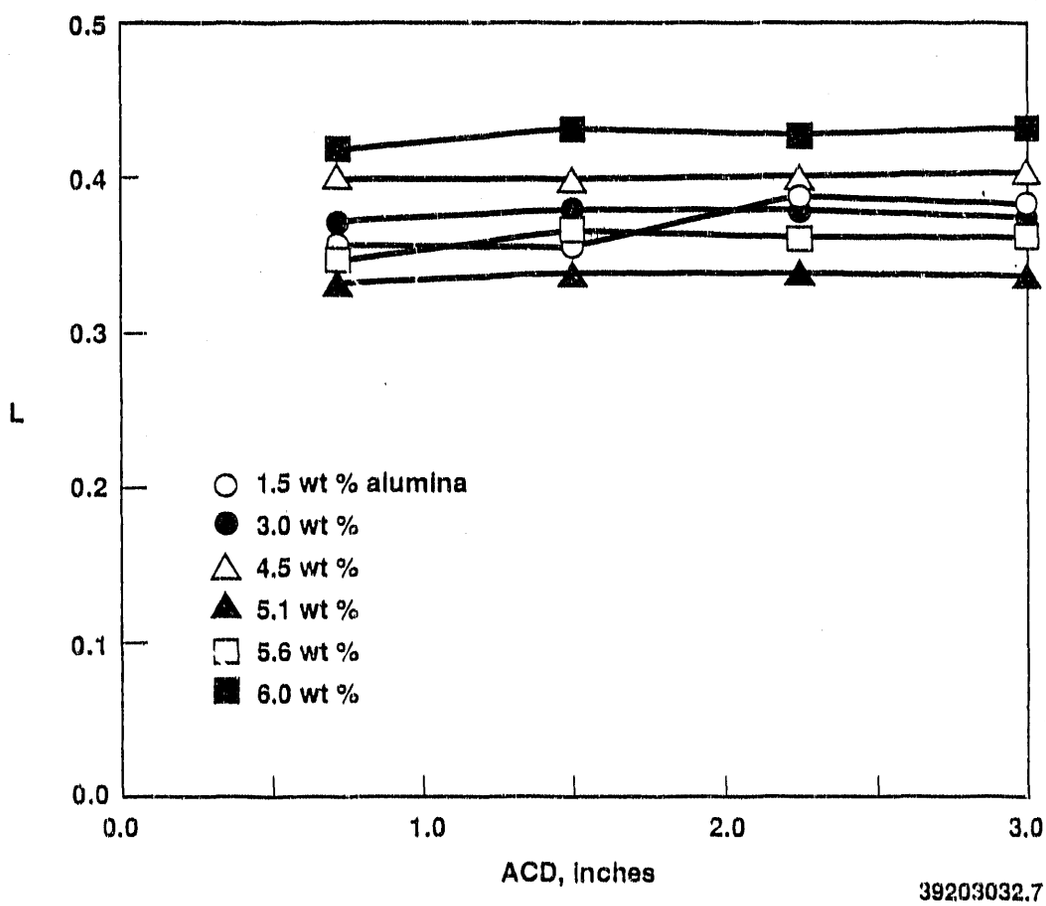

FIGURE 3.7. Plot of Conductance versus ACD for Various Alumina Concentrations. (ACD = 1.5 in.; a 10 Hz Ripple was Used.)

concentrations. The curves are essentially "flat," precluding any reliable determination of slopes and how they vary with alumina content. This sort of behavior was observed whenever ACD was varied.

It is not obvious why no dependency of any of the quantification parameters on ACD was observed given the apparent validity of Equation 3.5. The conductivity of cryolite decreases from about 2.8 to about 2.5 ohm^{-1} cm^{-1} at 1000°C when alumina concentration is increased from 0 to 6 wt% (Grjotheim 1982). A roughly 10% decrease should have been significant enough to measure in these laboratory tests. One possible explanation is that there were significant contributions to impedance from the electrode processes, particularly those involving the anode, and that the electrode effects obscured the relationships expected from the electrolyte alone. Another possibility is that the constant C′ was very small (or not constant) due to the actual relationship between K and the ACD for this cell geometry (i.e., fanning currents may have been significant even at the smaller ACD values). A very small (or variable) C′ might reduce the sensitivity of dX/d(ACD) below practicality. The latter possibility could be tested in a cell with a different geometry.

3.2 PILOT CELL TEST

Figure 3.8 shows a typical signal-versus-time plot for the current and voltage data collected during the pilot cell test. The most obvious feature in the data is the residual 360 Hz rectifier signal, which appears as a significant component of all of the signals even after filtering.

The following quantification parameters were determined from the current and voltage measurements during the pilot cell test: the conductance, L; the power ratio between the current and voltage, P; linear model parameters; and nonlinear model parameters. The various parameters were calculated using the total signals, the ac components, and the dc components of the signals. In addition, the correlation (magnitude squared coherence index) between the signals on the large carbon anode and each of the cermet anodes was determined

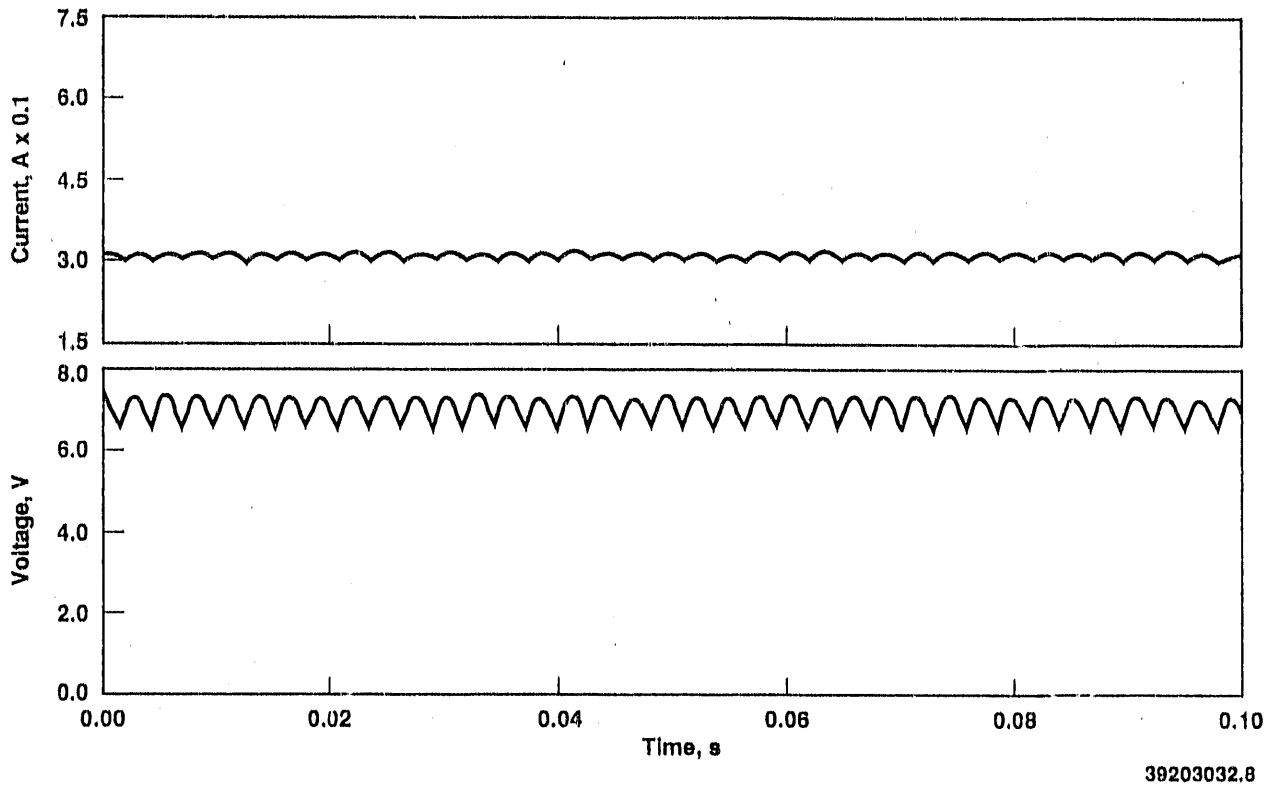

FIGURE 3.8. Typical Current and Voltage-versus-Time Plots for the Pilot Cell Test Data. (Data are from File PC51C and are for Anode in Position D at 23.1 Days.)

to see if there was any significant amount of coupling of the signals that would interfere with the analysis. A more complete description of the quantification parameters is given in the Appendix.

Because a large volume of signal data was collected during the pilot cell test, only some of it could be analyzed completely. Data from anodes in positions C, D, and F were selected for analysis. One of the reasons these positions were chosen was that they were occupied at the end of the pilot cell test when the alumina concentration was deliberately lowered. Data from these anodes therefore represented alumina concentrations over a wide rage of values, i.e., from 20% to 100% of alumina saturation. Since the objective of this study was to determine whether any correlation existed between the quantification parameters and the alumina concentration, the data from these anodes had the best chance of providing some indication of correlation (if

there was any at all). Sensitivity at high alumina concentrations (which is important for the cermet anodes) could be investigated in more detail once correlation over the much broader concentration range was demonstrated.

Preliminary analysis of the pilot cell data showed that the anodes in position C, D, and F seemed to behave differently in regards to how the quantification parameters varied with the alumina concentration. Upon initial inspection, the anodes in position D gave rise to signals that appeared to show some correlation with alumina concentration, while those in positions C and F showed no obvious behavior indicative of the alumina concentration. More careful examination of the signals from the anodes in position D, however, showed that even these did not correlate reproducibly with the alumina concentration. Certain unusual characteristics in the correlation plots reflected serious problems with attempting to correlate the signals from position D to alumina concentration without considering the effects of other operational parameters. It now appears likely that anodes in position D were plagued by the same effects that obscured sensitivity to alumina concentration for the rest of the cermet anodes in the pilot cell test. Some of the details of these interferences are discussed below.

Figure 3.9 shows the variation in L[a] as a function of time during the test for anodes in position D. (The behavior for the other quantification parameters for the same position is similar.) Also in the same figure is the plot of the variation of alumina concentration (expressed as percent of saturation) as a function of time during the test. (Recall that "0 days" corresponds to 8/3/91 at 1400 h.) As shown in Figure 3.9, there appears to be some tracking of the alumina concentration by L. For example, at about 13 days alumina concentration shows a dramatic drop and L drops dramatically also. During the period between 23 to 26 days, where alumina concentration drops (due to the deliberate stoppage of alumina feed), L is dropping also. In addition, as shown in the figure, there are numerous other instances

---

(a) The values for L are plotted using an arbitrary scale so that they overlap the alumina concentrations also plotted in these figures. Plots of the type were generated by Dr. C. L. Nikias to see if L (and the other quantification parameters) tracked the alumina concentration to any reasonable and consistent extent during the pilot cell test.

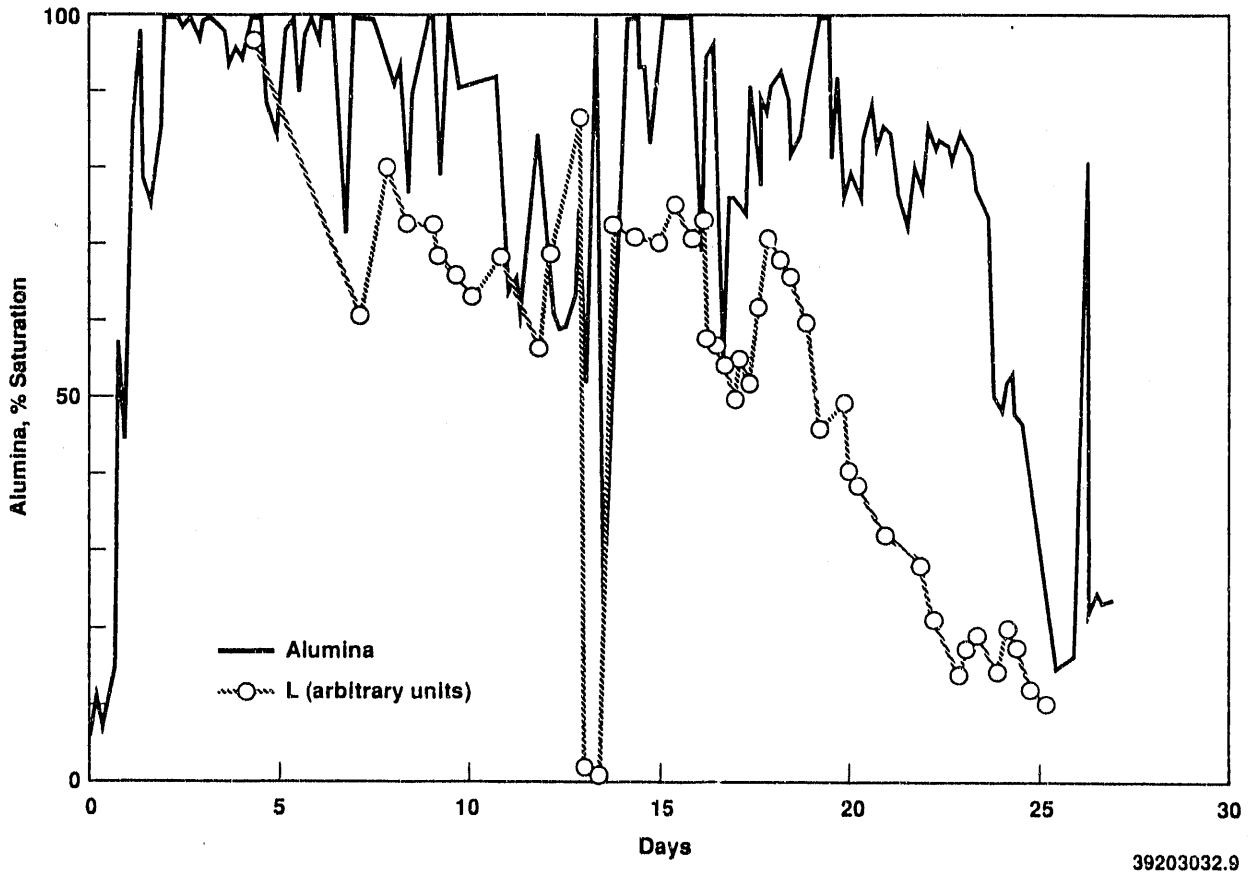

FIGURE 3.9. Comparison of L and Alumina Concentration as a Function of Time during the Pilot Cell Test for Anode in Position D

throughout the test where the value for L is observed to go down when alumina concentration goes down, or up when alumina concentration goes up.

Closer examination of the data in Figure 3.9, however, indicates there are some important discrepancies that cannot be explained at this time. Also, some of the operating conditions raise questions about even those situations where correlations seem promising. For example, the dramatic drop in L (and the other quantification parameters) at about 13 days occurs at precisely the time when the anode in position D was exchanged! (Refer to comments in Table 2.1.) Files PC17 through PC19, which contain the data that exhibited the drop, were collected between days 12.3 and 13.3 days, during which time

the anode in position D was being exchanged and therefore electrically disconnected. It appears that this drop in L and the other signal parameters is irrelevant in regards to alumina concentration, and, consequently, itsapparent correspondence to the observed drop in alumina concentration is completely fortuitous. The decrease in the value for L during the drop in alumina concentration between 23 and 26 days is also suspicious in that it actually begins earlier than the time at which the drop in alumina starts! L begins to drop even before day 20 when alumina is near its highest concentration. An alternative explanation for this drop in L may be the decrease in current through D that begins around day 20 (8/23/91) that is shown in Figure 2.8. The parameter L may be tracking current more closely than it is tracking alumina concentration.

In addition to the above-mentioned problems in the data analysis for the anodes in position D, there are numerous instances earlier on in the test when L and the alumina concentrations appear to show trends in opposite directions. For example, at measurements near days 10 and 12 in Figure 3.9, L goes down as the alumina concentration goes up. Clearly, the relationship between L (and the other quantification parameters) with alumina concentration for the anodes in position D, which seemed promising on first inspection, are not so promising under closer scrutiny and in light of variations in other cell conditions, especially the anode currents.

Anodes in positions C and F, whose signals show even poorer "correlation" with the alumina concentration give additional evidence that there is either very little sensitivity to alumina concentration or that fluctuations in other cell operating conditions are obscuring or reducing this sensitivity. Figure 3.10 shows a plot of L and alumina concentration for the anodes in position F, similar to the plot in Figure 3.9 for position D. Little, if any, meaningful relationship between the quantification parameter and alumina concentration is apparent from this figure. Similar lack of any correlation is observed for the other quantification parameters for both positions F and C.

Additional evidence for other cell operating conditions affecting the signals from the cermet anodes and possibly reducing their sensitivity to alumina concentration is shown in Figure 3.11. Figure 3.11 shows how the

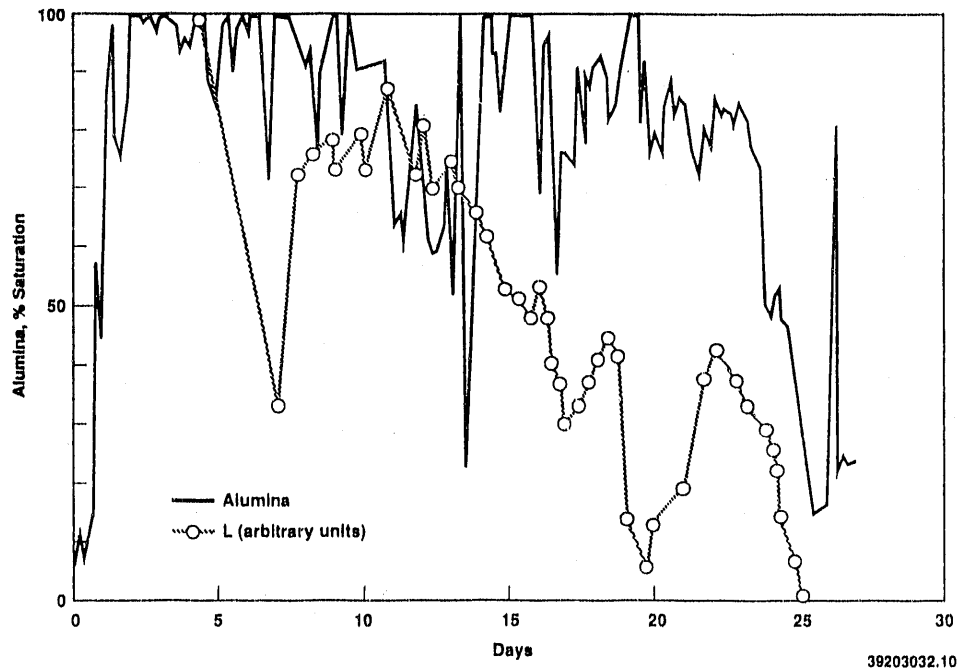

FIGURE 3.10. Comparison of L and Alumina Concentration as a Function of Time during the Pilot Cell Test for Anode in Position F

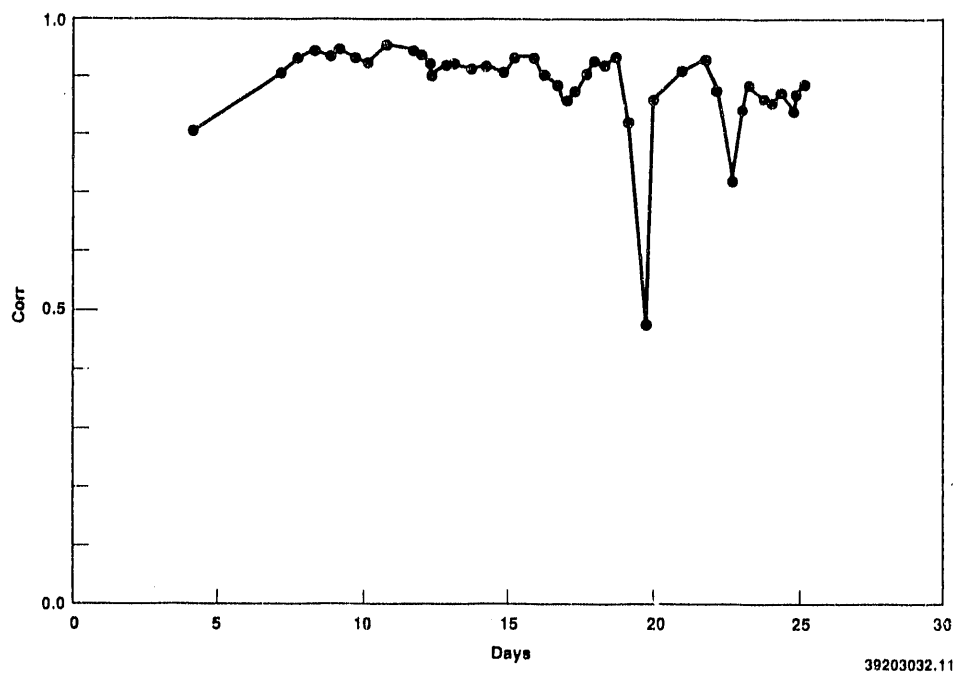

FIGURE 3.11. Correlation Plot for Anode in Position F with the Large Carbon Anode. Corr = 1000 x (Correlation Coefficient - 0.999).

correlation coefficient between the signals from the anodes in position F varied with those from the large carbon anode as a function of time during the test. (Anodes in other positions behaved similarly.) The correlation coefficient was very high (> 0.999) throughout the test (except at around day 20 which corresponds to a time when the anode in position F had very low currents and when it was being exchanged). The high correlation between these numbers suggests that there was a significant amount of coupling between the noise on the large carbon anode and the cermet anodes.[a] This coupling would be expected to confound any correlation with alumina concentration unless the twoanodes showed exactly the same response to alumina concentration, which is unlikely given what is known about the different characteristics of these anodes. (The "noise" signatures of carbon and inert anodes are known to be different due to the different sizes of the gas bubbles produced on them.)

(a) This coupling is not surprising given the large perturbing effect the carbon anode had on the dc voltages and currents at the cermet anodes. These perturbations and the ramifications on cermet anode performances are discussed in the forthcoming report on the results of the pilot cell test.

4.0 CONCLUSIONS AND RECOMMENDATIONS

The principal conclusion from this work is that none of the quantification parameters (derived from current and voltage signals from both laboratory and pilot-scale aluminum reduction cells using cermet anodes) have demonstrated sufficient and consistent sensitivity to alumina concentration to serve as a basis for an alumina sensor. There are two possible explanations for the lack of consistent correlation involving the quantification parameters: 1) there is no dependence, or a very weak one, on alumina concentration, and/or 2) there were overriding factors or extraneous noise that reduced the sensitivity or "overwhelmed" the signal components affected by alumina concentration. The latter possibility is most reasonable in light of the results from the pilot cell test that showed a dependence on anode current and the operation of the large carbon anode.

Based on the results of this work, it is recommended that further study using DSA methods be suspended or postponed until a less "noisy" pilot-scale test is performed with cermet anodes. Alternatively, a new strategy needs to be developed for applying the DSA approaches. For example, the methods could be applied to carbon anodes in commercial cells where a significantly greater volume of data can be collected over much longer times. A larger data base may facilitate the "factoring out" of the effects of fluctuations in other cell operating conditions.

5.0 REFERENCES

Grjotheim, K., C. Krohn, M. Malinovsky, K. Matiasovsky, and J. Thonstad. 1982. Aluminum Electrolysis. Aluminum-Verlag, Dusseldorf, FRG.

Skybakmoen, E., A. Solheim, and A. Sterten. 1990. "Phase Diagram Data in the System Na_3AlF_6-Li_3AlF_6-AlF_3-Al_2O_3 Part II: Alumina Solubility," from Light Metals 1990, The Minerals, Metals and Materials Society, Warrendale, Pennsylvania, pp. 317-324.

Windisch, C. F., Jr., O. H. Koski, N. D. Stice, C. L. Nikias, and L. G. Morgan. 1990. "Fiscal Year 1989 Annual Report for the Sensors Development Program." PNL-7309, Pacific Northwest Laboratory, Richland, Washington.

Windisch, C. F., Jr., T. R. Alcorn, A. T. Tabereaux. 1991. "Test Plan for the Pilot Cell Test of Inert Anodes: Report on the June 1991 Meeting at the Reynolds Metals Company Facility." PNL-7802, Pacific Northwest Laboratory, Richland, Washington.

APPENDIX[a]

DIGITAL SIGNAL ANALYSIS METHODS

(a) This Appendix was provided to the author in a personal communication from Dr. C. L. Nikias. Some of the notation in the Appendix is slightly different than in the text. In particular, note that L≡A for conductance, and COEF2 and COEF6 are denoted in the Appendix as two of the various a_i's.

MATHEMATICAL METHODS

A. Conductance Computation

The basic assumption here is that

$$I(n) = A \cdot V(n); \qquad n = 1, 2, \ldots, N \tag{1}$$

where A is the conductance ($1/R$ where R is resistance). Two methods have been employed to estimate A from the data, namely, the cross-correlation method and the average value method. The cross-correlation method gives estimate

$$A_{cc} = \sum_{n=1}^{N} I(n)V(n) \Big/ \sum_{n=1}^{N} V^2(n), \tag{2}$$

whereas the average value method

$$A_{AV} = \sum_{n=1}^{N} I(n) \Big/ \sum_{n=1}^{N} V(n). \tag{3}$$

B. Power Ratio Computation

The total power of current and voltage signals is respectively given by

$$\begin{aligned} P_I &= \frac{1}{N} \sum_{n=1}^{N} I^2(n) \\ P_V &= \frac{1}{N} \sum_{n=1}^{N} V(n)^2. \end{aligned} \tag{4}$$

Therefore, their ratio is

$$r_p = P_I \Big/ P_V. \tag{5}$$

C. Welch Method for Power Spectrum Estimation

This method is utilized not only to estimate the power spectrum of current/voltage signals but also to estimate their magnitude-squared coherence. Assuming that $\{Y(n)\}$, $n = 1, 2, \ldots, L$, is our data, the Welch method proceeds as follows.

1. Segment the data into K records of N samples each, i.e., L = KN. Assume that $\{X_i(n), n = 0, 1, \ldots, N-1\}$ is the data set per segment $i = 1, 2, \ldots, K$.
2. The periodogram spectrum is generated for each segment:

$$P_i(\ell) = FFT[X_i(n)]$$

and

$$S_i(\ell) = |P_i(\ell)|^2 \ for \ \ell = 0, 1, \ldots, \frac{N}{2} - 1$$

3. The Welch spectrum is obtained by averaging periodogram estimates:

$$S_{WE}(\ell) = \frac{1}{K} \sum_{i=1}^{K} S_i(\ell) \tag{6}$$

So, if $N = 2048$, then $\ell = 0, 1, \ldots, 1023$ spectral components are generated uniformly from 0 Hz - (1/2T) Hz where T is the sampling period of the data. It has been well-established in the literature [2], [3], that the variance of the Welch spectrum is

$$var[S_{WE}(\ell)] \sim \frac{1}{K} S^2(\ell)$$

where $S(\ell)$ is the true spectrum of the data and K the total number of segments. Thus, the larger is K, the smaller will be the variance in the spectrum estimate.

D. Magnitude-Squared Coherence (MSC)

The MSC is computed by utilizing the Welch method described above and two different sets of data, say $\{Y(1), \ldots, Y(L)\}$ and $\{Z(1), \ldots, Z(L)\}$. In particular, we have the following:

1. Segment both data into K records of N samples each; i.e., $L = K \cdot N$.
2. Let us assume that $\{x_i(n), n = 0, 1, \ldots, N-1\}$ is the data set per segment of $\{Y(k)\}$ and that $\{w_i(n), n = 0, 1, \ldots, N-1\}$ the data set per segment of $\{Z(k)\}$, where $i = 1, 2, \ldots, K$.

3. The FFT operation is applied on each segment of data

$$X_i(\ell) = FFT[x_i(n)],$$

$$W_i(\ell) = FFT[w_i(n)], \quad i = 1, 2, \ldots, K$$

and the auto- and cross-spectra generated; i.e.,

$$S_{xx}^{(i)}(\ell) = |X_i(\ell)|^2,$$

$$S_{ww}^{(i)}(\ell) = |W_i(\ell)|^2,$$

$$S_{xw}^{(i)}(\ell) = X_i(\ell) \cdot W_i^*(\ell), \quad \ell = 0, 1, \ldots, \frac{N}{2} - 1$$

4. The Welch auto- and cross-spectra are obtained by averaging

$$S_{xx}(\ell) = \frac{1}{K} \sum_{i=1}^{K} S_{xx}^{(i)}(\ell)$$

$$S_{ww}(\ell) = \frac{1}{K} \sum_{i=1}^{K} S_{ww}^{(i)}(\ell)$$

$$S_{xw}(\ell) = \frac{1}{K} \sum_{i=1}^{K} S_{xw}^{(i)}(\ell)$$

5. The magnitude-squared coherenced is defined by

$$MSC(\ell) = \frac{|S_{xw}(\ell)|^2}{S_{xx}(\ell) \cdot S_{ww}(\ell)} \tag{7}$$

$$\ell = 0, 1, \ldots, \frac{N}{2} - 1$$

and is always $0 \leq MSC(\ell) \leq 1$ for all frequency values ℓ.

E. Linear Modeling

A linear time-invariant finite impulse response (FIR) filter is assumed to relate the $I(n)$ and $V(n)$ of Figure 1, as follows.

$$I(n) = \sum_{i=0}^{M} a_i V(n-1) \tag{8}$$

where $\{a_o, a_1, \ldots, a_M\}$ are the parameters of the FIR model. Let us note that equation (8) is assumed when the dc value is subtracted from the signals and $V(n)$ is either 10Hz or 1kHz signal. The linear model parameters are estimated via cross-correlation operations and singular value decomposition.

From (8) we obtain the following relationship in the second-order statistics domain:

$$R_{IV}(\tau) = \sum_{i=0}^{M} a_i \quad R_{VV}(\tau + i) \tag{9}$$
$$\text{for } \tau = 0, 1, 2, \ldots J$$

where

$$R_{IV}(\tau) = \sum_{n} I(n)I(n+\tau) \qquad \text{autocorrelation}$$
$$R_{VV}(\tau + i) = \sum_{n} V(n-1)I(n+\tau). \qquad \text{cross} - \text{correlation} \tag{10}$$

From (9), we form the overdetermined system of equations

$$\begin{pmatrix} R_{VV}(0) & R_{VV}(1) & R_{VV}(2) & \ldots & R_{VV}(M) \\ R_{VV}(1) & R_{VV}(2) & R_{VV}(3) & \ldots & R_{VV}(M+1) \\ R_{VV}(2) & R_{VV}(3) & R_{VV}(4) & \ldots & R_{VV}(M+2) \\ \vdots & \vdots & \vdots & \vdots & \end{pmatrix} \begin{pmatrix} a_o \\ a_1 \\ a_2 \\ \vdots \\ a_M \end{pmatrix} = \begin{pmatrix} R_{IV}(0) \\ R_{IV}(1) \\ R_{IV}(2) \\ \vdots \end{pmatrix} \tag{11}$$
$$\mathbb{R} \quad \mathbb{a} \; = \; \mathbb{r}$$

where $\mathbb{R}$ is $(J+1) \times (M+1)$ matrix, $\mathbb{a} = [a_o, a_1, \ldots, a_M]^T$ and $\mathbb{r}$ is $(J+1) \times 1$ vector. The SVD of $\mathbb{R}$ is:

$$\mathbb{R} = \sum_{i=1}^{p} \sigma_i \mathbb{V}_i \mathbb{S}_i^H$$
$$\sigma_1 \geq \sigma_2 \geq \ldots \geq \sigma_p$$

where p is the rank of the matrix ($p \leq M+1$); σ_i are the singular values and "H" denotes transpose conjugate. The pseudo-inverse of the matrix $\mathbb{R}$ is

$$\mathbb{R}^+ = \sum_{i=1}^{p} \frac{1}{\sigma_i} S_i V_i^H \tag{12}$$

The solution $\mathbb{a}$ via SVD is given by

$$\mathbb{a} = \mathbb{R}^+ \mathbb{r}. \tag{13}$$

It is important to note that even if the matrix A is full rank ($p = M+1$), it can always be approximated by a lower rank matrix, $\hat{\mathbb{R}}$, in the mean-square error (mse) sense as follows

$$\hat{\mathbb{R}} = \sum_{i=1}^{q} \sigma_i \mathbb{V}_i \mathbb{S}_i^H \tag{14}$$

where $q < p$.

F. Nonlinear Modeling

A second-order Volterra model with linear and quadratic components is the following.

$$I(n) = \sum_{i=0}^{M} a_i V(n-i) + \sum_{i=0}^{2}\sum_{j=0}^{2} c(i,j)V(n-i)V(n-j) \tag{15}$$

where $\{a_o, \ldots, a_M\}$ are the linear component parameters and $\{c(0,0), c(1,1), c(2,2), c(0,1), c(0,2), c(1,2)\}$ are the nonlinear quadratic component parameters. Let us note that $c(i,j) = c(j,i)$. From (15), we have the following relationship between higher-order statistics of current and voltage:

$$R_{IV}(\tau) = \sum_{i=0}^{M} a_i R_{VV}(\tau+1) + \sum_{i=0}^{2}\sum_{j=0}^{2} c(i,j)M(\tau+i,\tau+j) \tag{16}$$

for $\tau = 0,1,2,3,\ldots J$, where

$R_{IV}(\tau), R_{VV}(\tau)$ are given by (10) and

$$M(\tau,p) = \sum_{n} V(n)V(n+\tau)V(n+p) \qquad \text{(third-order moments)} \tag{17}$$

From (16) we form an overdetermined system of equations and solve for $[a_o, a_1, \ldots, a_M, c(0,0), c(1,1), c(2,2), c(0,1), c(0,2), c(1,2),]$ using the singular value decomposition.

G. Quantification Parameters

The set of ad-hoc quantification parameters that has been identified from these DSA methods is the following:

1. Conductance between curren/voltage (A).
2. Power ratio between current/voltage (r_p).
3. Magnitude Square Coherence (MSC) as a function of frequency.
4. Bicoherence Index (to test whether or not there are quadratic nonlinearities in the relationship between current/voltage).
5. Power spectrum of current/voltage.
6. The linear model parameters and the singular values of R matrix.
7. The nonlinear model parameters and their corresponding singular values.

DISTRIBUTION

No. of
Copies

OFFSITE

M. J. McMonigle
U.S. Department of Energy
Office of Industrial Programs
Forrestal Building
Washington, DC 20585

P. H. Salmon-Cox
U.S. Department of Energy
Office of Industrial Programs
Forrestal Building
Washington, DC 20585

12 DOE Office of Scientific and
Technical Information

Dr. T. Alcorn
Manufacturing Technology
Laboratory
Reynolds Metals Co.
3326 East 2nd Street
Muscle Shoals, AL 35661-1258

C. Anderson
Columbia Aluminum Co.
85 John Day Dam Road
Goldendale, WA 98620

J. V. Anderson
WCVE3
EG&G Idaho, Inc.
Idaho Falls, ID 83415

D. Auburg
Bonneville Power Administration
P.O. Box 3621, PDX 97208
Portland, OR 97208

F. W. Baker
Ceramics Division
Alcoa Laboratories
Alcoa Center, PA 15069

No. of
Copies

M. Baltzell
Eastalco Aluminum Company
Alumax, Inc.
5601 Manor Woods
Frederick, MD 21701

J. A. Barclay
U.S. Bureau of Mines
2401 "E" Street N.W.
Washington, DC 20241

H. Robert Baumgartner
Ceramics Division
Alcoa Laboratories
Alcoa Center, PA 15069

T. R. Beck
Electrochemical Technology Corp.
1601 Dexter Avenue
Seattle, WA 98109

S. Berwagan
Bonneville Power Administration
P.O. Box 3621 K
Portland, OR 97208

T. M. Besmann
Metals and Ceramics Division
Oak Ridge National Laboratory
P.O. Box X, Bldg. 4515
Oak Ridge, TN 37831-6063

K. A. Blakely
President
Advanced Refractory
Technologies, Inc.
699 Hertel Ave.
Buffalo, NY 14207

M. H. Blenk
Du Pont
P.O. Box 787
Niagara Falls, NY 14302

No. of
Copies

L. G. Boxall
Martin Marietta Laboratories
1450 South Rolling
Baltimore, MD 21227

. Bracher
Kaiser Aluminum and Chemical
Corp.
825 N.E. Multnomah St.,
Suite 960
Portland, OR 97232-2150

R. Brandt
Department of Materials
Science and Engineering
University of Washington FB-10
Seattle, WA 98195

J. J. Brown, Jr.
Materials Engineering
Virginia Polytechnic Institute
Blacksburg, VA 24061

A. Budner
Bonneville Power Administration
P.O. Box 3621--EPA
Portland, OR 97208

A. J. Caputo
Development Division
Oak Ridge Y-12 Plant
Building 9202 MS-8095
Oak Ridge, TN 37831-8095

N. Clark
Bonneville Power Administration
Industrial Conservation
P.O. Box 3621
Portland, OR 97208

A. Cooke
Martin Marietta Laboratories
1450 South Rolling
Baltimore, MD 21227

No. of
Copies

J. A. Coppola
Standard Oil Engineered
Materials Company
P.O. Box 156
Niagara Falls, NY 14302

R. Curtis
Materials Development
Corporation
81 Hicks Avenue
Medford, MA 02155

J. V. Day
Kaiser Aluminum and Chemical
Corp.
E 2111 Hawthorne Road
Mead, WA 99021

D. H. DeYoung
Alcoa Technical Center
Alcoa Center, PA 15069

S. Diamond
Battelle Columbus Laboratories
505 King Avenue
Columbus, OH 43201-2693

T. Dwonch
Snake River District BPA
101 W. Poplar
Walla Walla, WA 99362

G. L. Eitel
Stone & Webster Engineering Corp
Greenwood Plaza Box 5406
Denver, CO 80217

R. Engdahl
Deposits and Composites, Inc.
318 Victory Drive
Herndon, VA 22070

No. of
Copies

J. F. Elliott
MIT
Room 4-138
77 Massachusetts Avenue
Cambridge, MA 02139

B. G. Epstein
A. D. Little, Inc.
955 Lenfant Plaza SW 4200
Washington, DC 20024-2119

J. W. Evans
University of California
Dept of Matl. Sci. and Mineral Eng.
Berkeley, CA 94720

R. A. Fenimore
ICI Advanced Materials
Rollins Building, Eighth Floor
Wilmington, DE 19897

D. A. Figgins
ARCO Petroleum Products Co.
P.O Box 61004
Anaheim, CA 92803-6104

P. Foster
Alcoa Laboratories
P.O. Box 772
New Kensington, PA 15068

J. Gee
Great Lakes Research Corp
P.O. Box 1031
Elizabethton, TN 37643

T. Gilligan
Eltech Systems Corp.
625 East Street
Fairport Harbor, OH 44077

W. M. Goldberger
Superior Graphite Co.
120 S. Riverside Plaza
Chicago, IL 60606

No. of
Copies

J. Goodwell
Center for Metals Production
Mellon Institute
4400 Fifth Avenue
Pittsburgh, PA 15213

Dr. Janet Gregg
Eltech Research Corporation
625 East Street
Fairport Harbor, OH 44077

J. A. S. Green
Martin Marietta Laboratories
1450 South Rolling
Baltimore, MD 21227

C. Griffin
Ceramatec Inc.
2425 S. 900 West
Salt Lake City, UT 84119

L. I. Grindstaff
Great Lakes Research Corp.
P.O. Box 1031
Elizabethton, TN 37643

J. Haggerty
MIT
Building 12, Room 009
77 Massachusetts Avenue
Cambridge, MA 02139

I. L. Harry
Electric Power Research Institute
P.O. Box 10412
Palo Alto, CA 94303

W. E. Haupin
2820 7th Street Road
Lower Burrell, PA 15068

R. Hill
Union Carbide Corp.
P.O. Box 94637
Cleveland, OH 44101

No. of
Copies

H. F. Hillegass
Alcoa Wenatchee Works
P.O. Box 221
Wenatchee, WA 98807

D. G. Howitt
College of Engineering
University of California, Davis
Davis, CA 95616

F. R. Huettig
Advanced Magnetics, Inc.
45 Corey Lane
Medham, NJ 07945

G. R. Hyde
U.S. Bureau of Mines
2401 "E" Street N.W.
Washington, DC 20241

S. C. Jacobs
Primary Processing
Aluminum Company of America
Alcoa Technical Center
Alcoa Center, PA 15069

S. H. Jan
Tennessee Valley Authority
R&D Division - MR 3A
Chattanooga, TN 37401

N. Jarrett
149 Jefferson Avenue
New Kinsington, PA 15068

J. Johnson
Intalco Aluminum Company
P.O. Box 937
Ferndale, WA 98248

L. Joo
Great Lakes Research Corp.
P.O. Box 1031
Elizabethton, TN 37643

No. of
Copies

M. Karmous
Oregon State Department of
Energy
625 Marion Street, N.E.
Salem, OR 97310

R. Keller
RD 3 Roundtop Road
Export, PA 15632

C. W. Koerr
The Stackpole Corporation
Cermag Division
201 Stackpole Street
St. Marys, PA 15847

K. Krupinski
Aristech Research
1000 Tech Center Dr.
Monroeville, PA 15146

G. Y. Lai
Cabot Corporation
P.O. Box 9013
Kokomo, IN 46902-9013

R. A. Landy
Director of Research
North American Refractories Co.
3127 Research Dr.
State College, PA 16801

J. E. Lane
Ceramic Research and
Development Center
Westinghouse Electric Corp.
1310 Beulah Road
Pittsburgh, PA 15235

Sai-Kwing Lau
Standard Oil Engineered
Materials Company
Niagara Falls R&D Center
P.O. Box 832
Niagara Falls, NY 14302

No. of
Copies

J. J. Leddy
Dow Chemical U.S.A.
1776 Building
Midland, MI 48640

W. W. Liang
Gas Research Institute
8600 West Bryne Mawr Avenue
Chicago, IL 60631

W. H. Link
Columbia Aluminum Corp.
85 John Day Dam Road
Goldendale, WA 98620

S. Loftness
Washington State Energy Office
400 E. Union
Olympia, WA 98504

W. Long
Building B815
Dow Chemical
Freeport, TX 77541

A. G. Longmuir
Kaiser Aluminum and Chemical
Corp.
P.O. Box 877
Pleasanton, CA 94566

R. A. Lowden
Metals and Ceramics Division
Oak Ridge National Laboratory
P.O. Box X, Bldg, 4515
Oak Ridge, TN 37831-6063

W. N. Maclay
Koppers Company, Inc.
1005 William Pitt Way
Pittsburgh, PA 15238-1336

J. C. McCloskey
Ten Mile River Associates
296 Mt. Hope Street
North Attleboro, MA 02760

No. of
Copies

Prof. G. Mamantov
University of Tennessee
Knoxville, TN 97996

S. C. Manaktala
Manager of Technology
Reduction Division
Kaiser Aluminum and Chemical
Corp.
300 Lakeside Drive
Oakland, CA 94643

V. H. Markant
Du Pont
P.O. Box 787
Niagara Falls, NY 14302

C. J. McMinn
Manufacturing Technology
Laboratory
Reynolds Metals Co.
3326 East 2nd Street
Muscle Shoals, AL 35661-1258

C. H. McMurtry
Standard Oil Engineered
Materials Company
Niagara Falls R&D Center
P.O. Box 832
Niagara Falls, NY 14302

M. A. Mitnick
Avco Specialty Materials
Subsidiary of Textron Inc.
2 Industrial Avenue
Lowell, MA 01851

H. Mortensen
R. Palika
Cercom, Inc.
P.O. Box 70
Vista, CA 92083

P. Ness
Washington State Dept of Trade
and Economic Development
2001 6th Avenue #2600
Seattle, WA 98121-2522

No. of
Copies

C. L. Nikias
30010 Via Borica
Rancho Palos Verdes, CA 90274

J. R. Payne
Kaiser Aluminum and Chemical
Corp.
P.O. Box 877
Pleasanton, CA 94566

T. Payne
Columbia Falls Aluminum Co.
Columbia Falls, MT

W. Pebley
Oregon Freeze Dry Corp.
525 25th Avenue SW
P.O. Box 1048
Albany, OR 97321

R. D. Peterson
Manufacturing Technology
Laboratory
Reynolds Metals Co.
3326 East 2nd Street
Muscle Shoals, AL 35661-1258

T. R. Pritchett
Kaiser Aluminum and Chemical
Corp.
P.O. Box 877
Pleasanton, CA 94566

W. W. Pritsky
Aluminum Association
900 19th St. N.W.
Washington, DC 20006

S. P. Ray
Alcoa Technical Center
Alcoa Center, PA 15069

Resource Center
Washington State Dept of Trade
and Economic Development
2001 6th Avenue #2700
Seattle, WA 98121-2522

No. of
Copies

J. F. Rhodes
Advanced Composite Materials
Corp.
1525 S. Buncomb Rd.
Greer, SC 29651

N. E. Richards
Manufacturing Technology
Laboratory
Reynolds Metals Co.
3326 East 2nd Street
Muscle Shoals, AL 35661-1258

J. J. Ritter
Ceramics Division
National Bureau of Standards
Gaithersburg, MD 20899

R. C. Rohwedder
3028 Ohio Street Longview, WAD.
R. Sadoway MIT Room 8-109
77 Massachusetts Avenue
Cambridge, MA 02139

W. Scott
Department of Materials
Science & Engineering
Wilcox Hall FB-10
University of Washington
Seattle, WA 98195

D. R. Secrist
Great Lakes Research Corp.
P.O. Box 1031
Elizabethton, TN 37643

A. B. Shah
Noranda Aluminum, Inc.
P.O. Box 70
New Madras, MO 36869

N. Shelton
Intalco
1300 S.W. 5th, Suite 3508
Portland, OR 97201

No. of
Copies

Brian Spector
Pace Consultants
4848 Loop Central Drive
Houston, TX 77081

F. W. Spillers
Dow Chemical U.S.A.
B-1210 Building
Freeport, TX 77541

Dr. Richard M. Spriggs
Office of the Director
Center for Advanced
Ceramic Technology
Alfred University
Alfred, NY 14802

D. V. Stewart
Manufacturing Technology
Laboratory
Reynolds Metals Co.
3326 East 2nd St.
Muscle Shoals, AL 35661-1258

D. Strahan
Reynolds Metals Company
P.O. Box 27003
Richmond, VA 23261

A. T. Tabereaux
Manufacturing Technology
Laboratory
Reynolds Metals Co.
3326 East 2nd Street
Muscle Shoals, AL 35661-1258

G. P. Tarcy
Aluminum Company of America
Alcoa Technical Center
Alcoa Center, PA 15069

P. Thaure
Alumax, Inc.
5655 Peachtree Parkway
Norcross, GA 30092

No. of
Copies

W. H. Thielbahr
Conservative Technology
Division
DOE-Idaho Operations Office
785 DOE Place
Idaho Falls, ID 83402

S. Thomson
General Manager
Klickitat PUD
1313 S. Columbus
Goldendale, WA 98620

R. Unger
Merner Research
P.O. Box 248
Ridgewood, NJ 07451

A. Vinnard
Bonneville Power
Administration (KWI)
P.O. Box 3621
Portland, OR 97208

T. Von Muller-KWI
Bonneville Power Administration
P.O. Box 3621
Portland, OR 97208

D. H. Weinblatt
AIMCOR
One Parkway North
Deerfield, IL 60015

J. D. Weyand
EG&G Idaho, Inc.
Idaho Falls, ID 83415

B. Wilcox
Northwest Aluminum Co.
3313 W. Second St.
The Dalles, OR 97058

C. B. Wilson
Dow Chemical U.S.A.
Texas Operations
B-101 Building
Freeport, TX 77541

No. of
Copies

FOREIGN

D. Brodie
Comalco Ltd.
55 Collins St.
Melbourne,
AUSTRALIA

H. Connor
Group Licensing Controller
Johnson Matthey, plc
New Garden House
78 Hatton Garden
London EC1N 8JP
ENGLAND

T. Kjar
Comalco Ltd.
55 Collins St.
Melbourne,
AUSTRALIA

E. W. Dewing
Alcan International
P.O. Box 8400
Kingston, Ontario
CANADA K7L 4Z4

D. N. MacMillan
Alcan International
C.P. 1250
Jonquieve, Quebec
CANADA G7S 4K8

A. Oye
Institute of Inorganic
Chemistry
Norwegian Institute of
Technology
University of Trondheim
N-7034 Trondheim-NTH,
NORWAY

No. of
Copies

J. Thonstad
Laboratories of Industrial
Electrochemistry
Norwegian Institute of
Technology
University of Trondheim
N-7034 Trondheim-NTH,
NORWAY

K. O. Vee
ASV Ardal Verk
N-5875 Ardalstargen,
NORWAY

Dr. Eric Frazer
CSIRO Australia
Division of Mineral Products
339 Williamstown Road
P.O. Box 124
Port Melbourne, Vic 3207

ONSITE

DOE Richland Field Office

D. R. Segna

24 Pacific Northwest Laboratory

M. Clement
D. K. Hilliard
G. L. McVay
N. L. Moore
L. G. Morgan
D. M. Strachan
R. W. Westerman
R. E. Williford
C. F. Windisch (10)
Publishing Coordination
Technical Report Files (5)

END

DATE FILMED

6/12/92